Synthesis and Functions of New Block Copolymers Possessing Dense Triazole Blocks

A Doctoral Thesis

by

Yanqiong Yang

Submitted to

The Graduate School of Science, Osaka University

August 2019

Acknowledgement

This work was carried out from 2016 to 2019 under the supervision of Professor Akihito Hashidzume at the Department of Macromolecular Science, Graduate School of Science, Osaka University. I would like to express my sincerest gratitude to Professor Akihito Hashidzume for his kindest guidance and assistance throughout this study. I also would like to express my deep gratitude to Assistant Professor Yuri Kamon for her helpful advice and discussions.

I would like to express my deep gratitude to Professor Sadahito Aoshima, Professor Tadashi Inoue, and Professor Takahiro Sato for their careful review and valuable comments. I also would like to express my gratitude to Professor Yoshinori Takashima, Associate Professor Arihiro Kanazawa, Associate Professor Osamu Urakawa at Osaka University for their kind support on some measurements and suggestions.

This work is partly financial-supported by Sasakawa Scientific Research Grant from the Japan Science Society. Many thanks!

I would like to express my deep gratitude Professor Sadahito Aoshima again at Osaka University, and Professor Nathaniel A. Lynd at the University of Texas

at Austin for their kind support on my stay at the University of Texas at Austin for two months. The small angle scattering measurements in this work were conducted at the University of Texas at Austin with the kind help from Mr. Paul W. Meyer.

A special gratitude extends to Professor Françoise M. Winnik at University of Helsinki for her helpful suggestions and valuable discussions on this work. Many thanks!

Many thanks to all the group members of Hashidzume laboratory for their continuous help and warmest friendship. I appreciate the financial support from Japanese Government, MEXT (Ministry of Education, Culture, Sports, Science and Technology) (October, 2016-present).

Finally, sincerest thanks to my parents and friends for their constant support and warmest encouragements.

August 2019

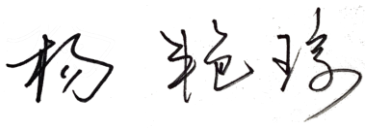

Yanqiong Yang

Contents

Chapter 1

General Introduction

1-1. Fundamental Properties of 1,2,3-Triazole Moieties

1,2,3-Triazole is a nitrogen-rich functional group composed of three nitrogen and two carbon atoms, as show in Figure 1-1. It is an intriguing functional group, in which the carbon atoms and the nitrogen atom on the 1-position are expected to be positively charged, while the 2- and 3-nitrogen atoms show negative partial charges.[1,2] On the basis of the relevant contributing structures and inductive effects, 1,2,3-triazole ring has various advantageous properties.

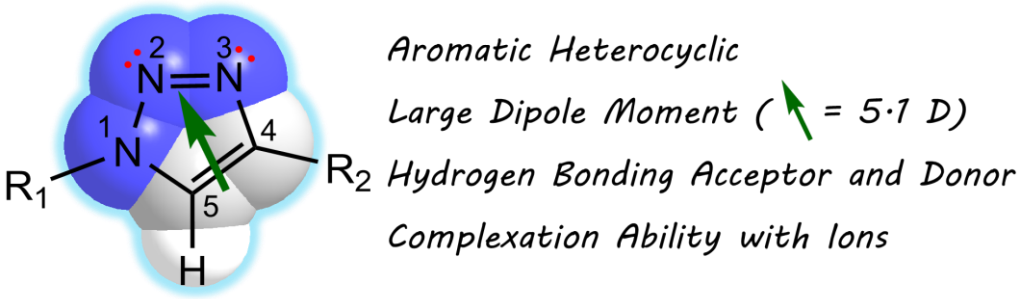

Figure 1-1. Structural features of 1,2,3-triazole moiety.

Firstly, it has high chemical stability,[3,4] that is inert against oxidation, reduction, and hydrolysis even under acidic or basic conditions, in all solvents,

and in the presence of various functional groups.[5,6] Secondly, it has a very large dipole moment.[7-9] The three nitrogen atoms of the 1,2,3-triazole located together cause a strong polarization of the aromatic system and the σ framework, so that a large dipole moment is produced by this unique structure.[1,10] Therefore, 1,2,3-triazole moiety can interact with polar molecules through dipole–dipole interaction.

Moreover, 1,2,3-triazole can also form hydrogen bonding.[11,12] The two different lone pairs on the N atoms can act as hydrogen bonding acceptor, but the ability of hydrogen bonding formation of these two N atoms is different. A theoretical calculation suggests that the N-3 lone pair has a higher basicity than does the N-2 one in the gas phase, indicating that the N-3 lone pair is a stronger hydrogen bonding acceptor.[13] It should be noted here that 1,2,3-triazole may act as a potent hydrogen bond donor as well, because the extrinsic polarization of carbon atom can afford hydrogen bonds involving the C–H group that may be as strong as for classical, intrinsically polarized hydrogen bond donors (N–H and O–H).[14-16] From the 1,2,3-triazole ring structure, it can be seen that the large dipole moment is almost aligned with the C–H bond. Therefore, the relatively high CH-acidity on the 5C-position qualifies the 1,2,3-triazole as a potent hydrogen bonding donor.

Finally, in combination with the relatively high CH-acidity on the C5-

position and the lone pair on basic N-2 and N-3, 1,2,3-triazole is a good noncovalent interaction site through coordination bonding with metal ions[17–20] and complexation with anion through (charge-assisted) hydrogen bonds. [21–24]

Scheme 1-1. Formation of 1,2,3-triazoles.

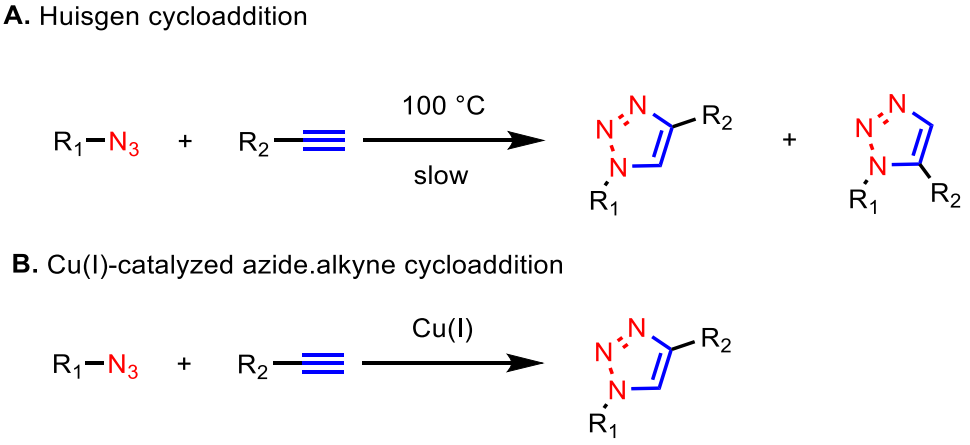

1-2. Huisgen Reaction to CuAAC Reaction

Concerning the preparation of 1,2,3-triazle ring, reactions that inevitably need to know are Huisgen cycloaddition[25-27] and copper(I)-catalyzed azide–alkyne cycloaddition (CuAAC) reaction, especially CuAAC. CuAAC has been reported by Sharpless[28] and Meldal et al.[29] in 2002. Before the reporting of CuAAC in 2002, 1,2,3-triazole was synthesized by the non-catalyzed azide/alkyne reaction (Huisgen cycloaddition). Compared with CuAAC, Huisgen cycloaddition is a slow and unselective process which produces a mixture of 1,4 and 1,5-

disubstituted products.[30,31] Whereas, due to the application of copper(I) species in CuAAC, this 1,3-dipolar cycloaddition reaction is markedly accelerated, which proceeds highly efficient in various solvents, including water, even in the presence of a wide variety of functional groups. Another significant advantage of CuAAC compared to Huisgen cycloaddition is that CuAAC selectively produces 1,4-disubstituted 1,2,3-triazoles instead of a mixture of 1,4 and 1,5-disubstitution products, as shown in Scheme 1-1.

Thus, CuAAC has become one of the most important "click" reactions. It has been widely employed in a variety of fields ranging from biorelated chemistry[32–36] to materials science.[37–40] CuAAC has been also applied to polymer chemistry, e.g., elongation of the main chain,[41] side chain modification,[42] cyclization,[43] cross-linking,[44] and the formation of dendrimers and hyper-branch polymers.[45–47] However, most of these studies, so far, deal with the 1,2,3-triazole moiety just as a simple, 'non-interfering' linker to connect two independent molecular or macromolecular species together, and the properties of the formed 1,2,3-triazole unit and the properties of polymer composed of 1,2,3-triazole moieties have been scarcely addressed.

1-3. Triazole-Based Functional Polymers

As mentioned above, 1,2,3-triazole is actually an interesting heterocycle. It

can offer diverse supramolecular interactions, e.g., hydrogen bonding with protic compounds, coordination bonding with ions, π–π stacking, and dipole–dipole interaction.[48,49] However, the researches on triazole-based functional polymers are still at elementary level. One main reason for this situation should be the difficult preparation of 1,2,3-triazoles before the development of CuAAC reaction. Therefore, since the development of CuAAC, which provides a highly efficient modular synthetic strategy to prepare triazole moiety, more and more researchers have been attracted to explore 1,2,3-triazole-based new functional materials.

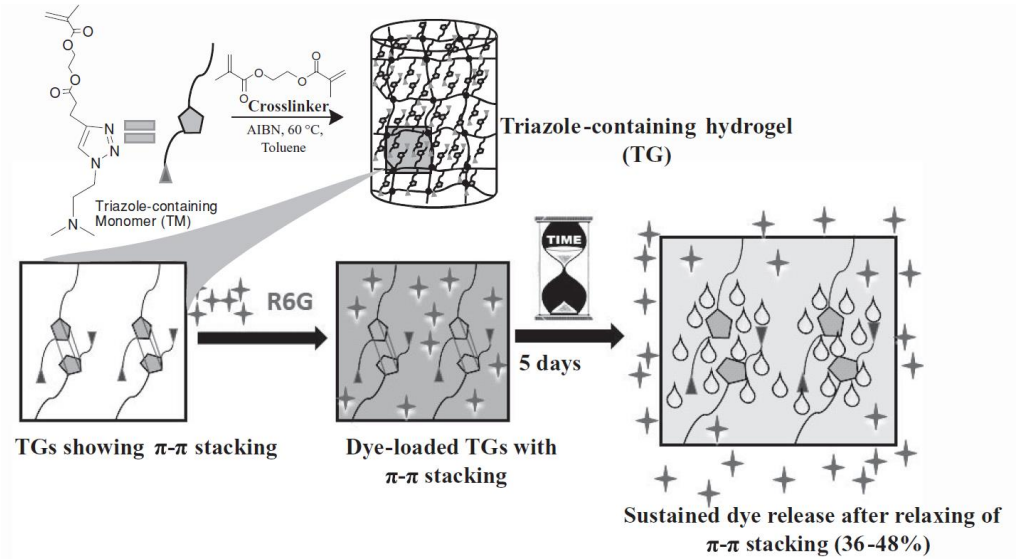

Figure 1-2. Triazole-containing hydrogels and their sustained swelling and drug release behaviors. Reprinted with permission from ref. 51. Copyright 2013 WILEY–VCH.

At present, some examples have been reported on functional polymers by utilizing the properties of 1,2,3-triazole units. These polymers were utilized for gelation, sensing, and control of clouding point of thermosensitive polymers, controlled release of drugs, and tough network polymers.[50–56] For example, Lee et. al[51] prepared triazole-containing hydrogels. Because of the π–π stacking of triazole rings in the side chain, the hydrogels showed continuous swelling up to 7 days and sustained model drug release properties (Figure 1-2).

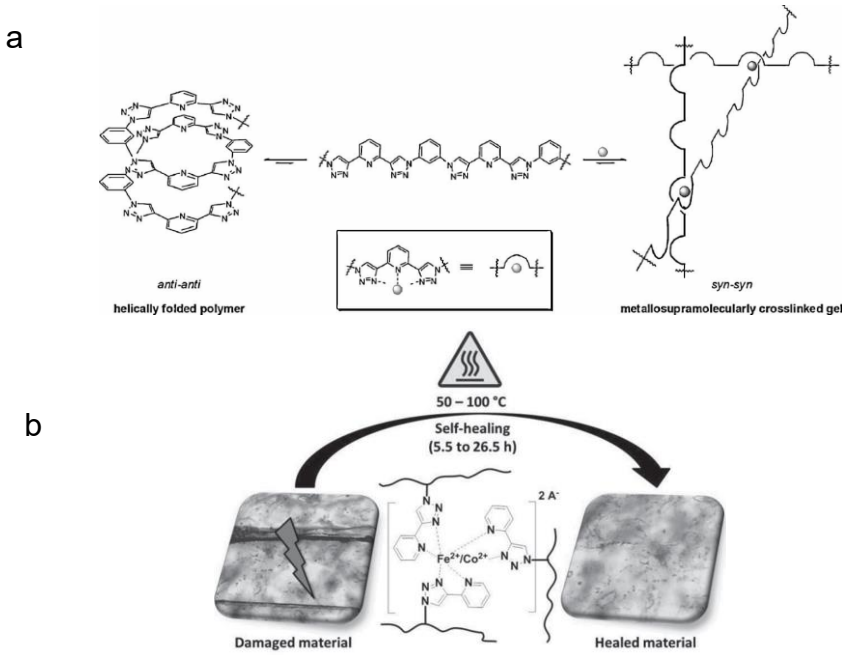

Figure 1-3. Metallosupramolecularly crosslinked gels (a), and triazole-pyridine-based self-healable metallopolymers (b), via metal–ligand interactions. Reprinted with permission from refs. 50 (a) and 56 (b). Copyright 2008 (a) and 2015 (b) WILEY–VCH.

Hecht et al.[50] prepared helical triazole-pyridine/benzene copolymers using 2,6-bis(1,2,3-triazol-4-yl) pyridines as building blocks. Utilizing the main chain of these copolymers as ligands for transition metal ions, metallosupramolecularly crosslinked gels were prepared (Figure 1-3a). Schubert and coworkers[56] reported triazole-pyridine-based self-healable metallopolymers via metal–ligand interactions between attached bidentate triazole-pyridine ligands with Fe(II) and Co(II) salts (Figure 1-3b).

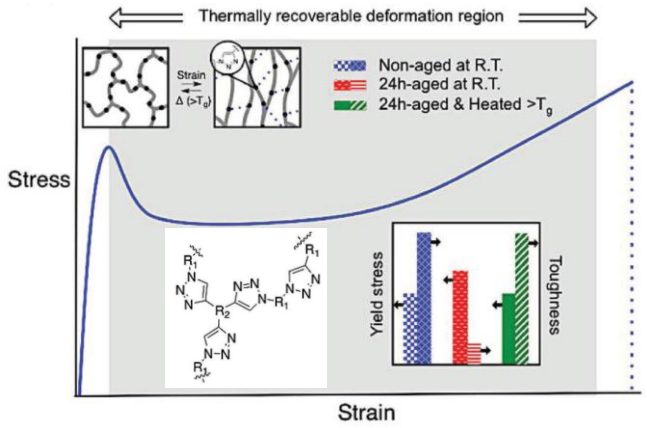

Figure 1-4. Cross-linked triazole-containing networks and noncovalent interactions of the triazole rings. Reprinted with permission from ref. 57. Copyright 2018 WILEY–VCH.

Very recently, Bowman and coworkers[57] prepared flexible and sterically hindered triazole-based glassy polymer networks. The sterically hindered triazole-based networks show dramatically enhanced toughness, elongation to

break, and tensile strength based on the in-situ formation of the noncovalent interactions of the rigid triazole rings and freely rotational bonds between network junctions (Figure 1-4).

To date, an increasing number of researchers are taking part in the exploration of triazole-based functional polymers. However, in these poly(triazole)s, the triazole units are generally separated by relatively longer spacer or sparsely distributed in polymer side chains.[52–58] These triazole units cannot efficiently interact with each other either because they enjoy a higher degree of conformational freedom on the side chain or because they are located too far away from each other. Hence, the function of triazoles would be eclipsed. As for the network cross-linked, hyperbranched-linked, and dendritic-linked compounds, the triazole units are anchored within a rigid structure framework. Therefore, almost no conformational freedom was allowed for the generation of ordered structures.

Recently, Hashidzume et al.[59] carried out the polymerization of 3-azido-1-propyne (AP) and 3-azido-1-butyne (AB) by CuAAC polymerization and obtained oligomers composed of dense 1,2,3-triazole moieties in the backbone (Scheme 1-2). To the best of the author's knowledge, these oligomers possess the densest 1,2,3-triazole moieties. These AP and AB oligomers exhibited significantly strong inter/intramolecular interactions. This observation indicates that polymers composed by dense triazoles are highly promising as new functional

polymers. However, the strong inter/intramolecular interaction also caused a problem that is poor solubility. The oligomers are only soluble in strong acids, e.g., concentrated hydrochloric acid, sulfuric acid, and nitric acid, but are insoluble in water and all the organic solvents examined. Investigation on the properties of these dense triazole-based polymers is an important challenge.

Scheme 1-2. Structures of oligomers composed of dense 1,2,3-triazole moieties.[59]

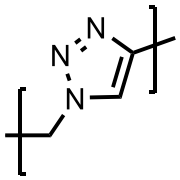

poly(3-azido-1-propyne)
(PAP)

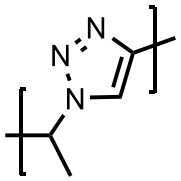

Poly(3-azido-1-butyne)
(PAB)

1-4. Block Copolymers

Block copolymers (BCPs) represent an important class of microstructurally engineered materials in large quantity because their properties can be systematically controlled by tuning the macromolecular structure, chain architecture, and relative block lengths.[60] One of the most intriguing points of block copolymers is that on one hand these polymers can efficiently combine the

properties of each blocks, and, on the other hand, the unique structure and properties of the individual blocks are almost maintained. Up to now, numerous advanced BCPs with specific properties suitable for targeted application have been prepared.[60–62]

Owning to the excellent chain structure of block copolymers, it is believed that by incorporating the correct type of functional group partners or segments with the dense oligo- and poly(triazole) backbone, novel supramolecular dense triazole-based functional polymer can be created.

1-5. Scope of This Thesis

The aim of this work is to synthesize dense triazole-based block copolymers, which are well soluble and processable, and to investigate their properties and application as new functional materials.

Chapter 2 presents the synthesis of a new type of diblock copolymers possessing a dense 1,2,3-triazole block by CuAAC polymerization. The author has chosen poly(ethylene glycol) (PEG) as a well-soluble and thermoresponsive block, and synthesized a series of diblock copolymers, poly(ethylene glycol)-*b*-poly(3-azido-1-propyne) (EG*m*-*b*-AP*n*) and poly(ethylene glycol)-*b*-poly(3-azido-1-butyne) (EG*m*-*b*-AB*n*), where *m* and *n* denote the degrees of polymerization of PEG and dense 1,2,3-triazole blocks, respectively. The block copolymer samples

obtained are well soluble in water. Their association behavior and thermoresponsive properties in aqueous solution are systematically investigated. The block copolymers self-assemble into various nanostructures, i.e. spherical micelles, vesicles, and cylindrical micelles, depending on the relative length of blocks. Aqueous solutions of these assemblies undergo lower critical solution temperature (LCST)-type phase separation. The thermoresponsive association behavior can be controlled by adjusting the ratio of block lengths and by attaching methyl substituents.

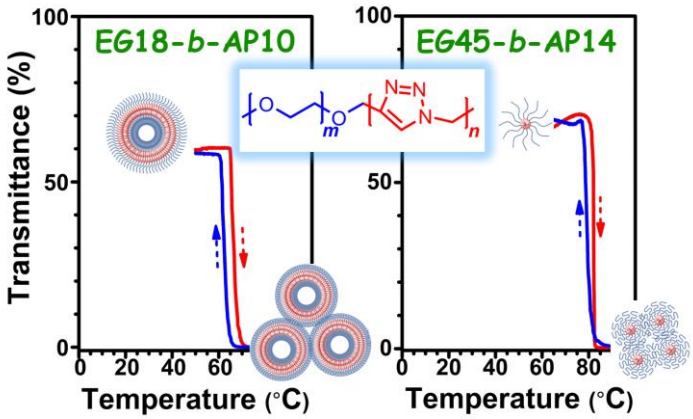

Figure 1-5. Typical illustration of the EG*m*-*b*-AP*n* aggregates formed and their thermoresponsive behavior.

Chapter 3 reveals the novel photophysical properties of the diblock copolymers in different solvents. A new type of dense triazole-based fluorescent polymers are developed. The author systematically studies the absorption and

emission properties of the block copolymers. The experimental data have exhibited that AP*n* block is an intrinsic fluorophore. The emission of EG*m*-*b*-AP*n* can be easily tuned from ultraviolet to green fluorescence by changing the excitation wavelength. This enables fine-tuning of its optical property without the need of changing the chromophore. Moreover, the block copolymers show a fluorescence response to metal ions, e.g., Cu^{2+}.

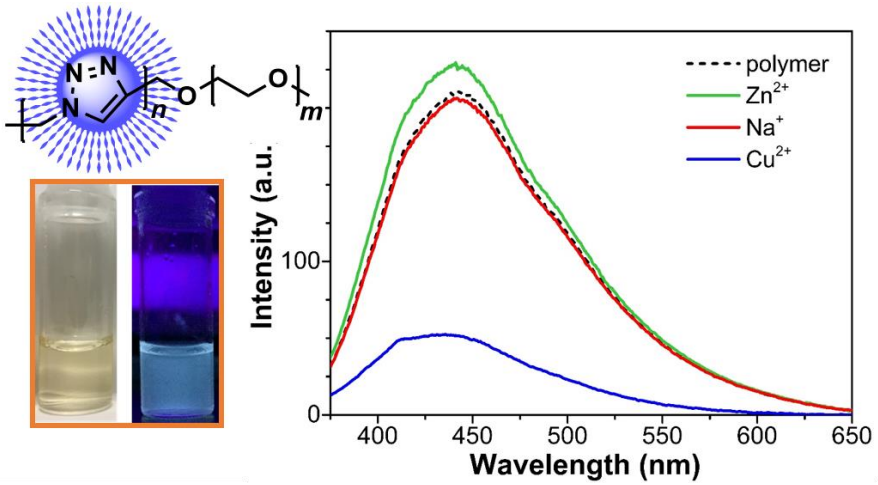

Figure 1-6. Optical picture of emission and the effect of metal ions on fluorescence.

Chapter 4 describes a new class of BAB-type triblock copolymers, consisting of the middle PEG and terminal dense 1,2,3-triazole blocks. Because of the strong supramolecular interaction of triazole blocks, the block copolymers form a strong

and tough network structure that provides excellent tensile mechanical properties and efficient healability. A series of triblock copolymers with different relative length are prepared. The detail nanostructure of the networks and the effect of relative length on the mechanical property and self-healing properties are investigated.

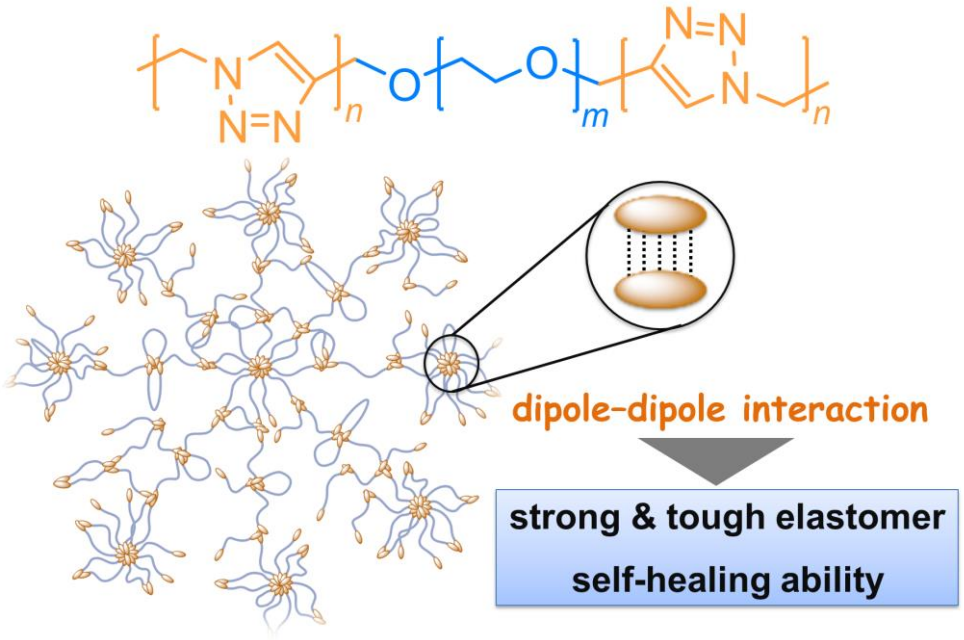

Figure 1-7. Illustration of the network structure of the elastomer formed by triblock with dynamic dipole–dipole interaction and microphase separation.

The main findings and conclusions from this research are summarized in Chapter 5.

References

(1) Adam, W.; Grimison, A. *Theor. Chim. Acta* **1967**, *7*, 342–351.

(2) Jug, K.; Chiodo, S.; Calaminici, P.; Avramopoulos, A.; Papadopoulos, M. G. *J. Phys. Chem. A* **2003**, *107*, 4172–4183.

(3) Cassidy, M. P.; Raushel, J.; Fokin, V. V. *Angew. Chem., Int. Ed.* **2006**, *45*, 3154–3157.

(4) Horneff, T.; Chuprakov, S.; Chernyak, N.; Gevorgyan, V.; Fokin, V. V. *J. Am. Chem. Soc.* **2008**, *130*, 14972–14974.

(5) Kolb, H. C.; Sharpless, K. B. *Drug Discovery Today* **2003**, *8*, 1128–1137.

(6) Bock, V. D.; Hiemstra, H.; van Maarseveen, J. H. *Eur. J. Org. Chem.* **2005**, *1*, 51–68.

(7) Begtrup, M.; Nielsen, C. J.; Nygaard, L.; Samdal, S.; Sjogren, C. E.; Sorensen, G. O. *Acta Chem. Scand., Ser. A* **1988**, *42*, 500–514.

(8) Jug, K.; Chiodo, S.; Calaminici, P.; Avramopoulos, A.; Papadopoulos, M. G. *J. Phys. Chem. A* **2003**, *107*, 4172–4183.

(9) Abboud, J. L. M.; Foces-Foces, C.; Notario, R.; Trifonov, R. E.; Volovodenko, A. P.; Ostrovskii, V. A.; Alkorta, I.; Elguero, J. *Eur. J. Org. Chem.* **2001**, *16*, 3013–3024.

(10) Oziminski, W. P.; Dobrowolski, J. C.; Mazureka, A. P., *J. Mol.*

Struct. **2003**, *651*, 697–704.

(11) Horne, W. S.; Yadav, M. K.; Stout, C. D.; Ghadiri, M. R. *J. Am. Chem. So.* **2004,** *126*, 15366–15367.

(12) Fisher, M. G.; Gale, P. A.; Hiscock, J. R.; Hursthouse, M. B.; Light, M. E.; Schmidtchen, F. P.; Tong, C. C. *Chem. Commun.* **2009**, *21*, 3017–3019.

(13) Abboud, J. L. M.; Foces-Foces, C.; Notario, R.; Trifonov, R. E.; Volovodenko, A. P.; Ostrovskii, V. A.; Alkorta, I.; Elguero, J. *European J. Org. Chem.* **2001**, *16*, 3013–3024.

(14) Bryantsev, V. S.; Hay, B. P. *Org. Lett.* **2005**, *7*, 5031–5034.

(15) McDonald, K. P.; Hua Y.; Flood, A. H. *Top. Heterocycl. Chem.* **2010**, *24*, 341–366.

(16) Hay, B. P.; Bryantsev, V. S, *Chem. Commun.* **2008**, *21*, 2417–2428.

(17) Ghosh, K.; Panja, A.; Panja, S. *New J. Chem.* **2016**, *40* , 3476–3483.

(18) Felici, M.; Contreras-Carballada, P.; Smits, J. M. M.; Nolte, R. J. M.; Williams, R. M.; De Cola, L.; Feiters, M. C. *Molecules* **2010**, *15*, 2039–2059.

(19) Kumar, A.; Pandey, P. S., *Tetrahedron Lett.* **2009**, *50*, 5842–5845.

(20) Noor, A.; Lewis, J. E. M.; Cameron, S. A.; Moratti, S. C.; Crowley, J. D. *Supramol. Chem.* **2012**, *24*, 492–498.

(21) Hua, Y. R.; Flood, A. H. *J. Am. Chem. Soc.* **2010**, *132*, 12838–12840.

(22) Li, Y. J.; Flood, A. H. *Angew. Chem., Int. Ed.* **2008**, *47*, 2649–2652.

(23) White, N. G.; Beer, P. D. *Chem. Commun.* **2012**, *48*, 8499–8501.

(24) Garcia, F.; Arago, J.; Viruela, R.; Orti, E.; Sanchez, L. *Org. Biomol. Chem.* **2013**, *11*, 765–772.

(25) Huisgen, R. *Angew. Chem., Int. Ed.* **1963**, *2*, 565–598.

(26) Huisgen, R. *Angew. Chem., Int. Ed.* **1963**, *2*, 633–645.

(27) Huisgen, R. *Angew. Chem., Int. Ed.* **1968**, *7*, 321–328.

(28) Rostovtsev, V. V.; Green, L. G.; Fokin, V. V.; Sharpless, K. B. *Angew. Chem., Int. Ed.* **2002**, *41*, 2596–2599.

(29) Tornoe, C. W.; Christensen, C.; Meldal, M. *J. Org. Chem.* **2002**, *67*, 3057–3064.

(30) Huisgen, R. *J. Org. Chem.* **1968**, *33*, 2291–2297.

(31) Huisgen, R. *J. Org. Chem.* **1976**, *41*, 403–419.

(32) Hong, V.; Presolski, S. I.; Ma, C.; Finn, M. G. *Angew. Chem., Int. Ed.* **2009**, *48*, 9879–9883.

(33) Sokolova, N. V.; Nenajdenko, V. G. *Rsc Adv.* **2013**, *3*, 16212–16242.

(34) Holub, J. M.; Kirshenbaum, K. *Chem. Soc. Rev.* **2010**, *39*, 1325–1337.

(35) Shie, J. J.; Liu, Y. C.; Lee, Y. M.; Lim, C.; Fang, J. M.; Wong, C. H. *J. Am. Chem. Soc.* **2014**, *136*, 9953–9961.

(36) Li, X. C. *Chem. Asian J.* **2011**, *6*, 2606–2616.

(37) Shieh, P.; Dien, V. T.; Beahm, B. J.; Castellano, J. M.; Wyss-Coray, T.; Bertozzi, C. R. *J. Am. Chem. Soc.* **2015**, *137*, 7145–7151.

(38) Qin, G. T.; Santos, C.; Zhang, W.; Li, Y.; Kumar, A.; Erasquin, U. J.; Liu, K.; Muradov, P.; Trautner, B. W.; Cai, C. Z. *J. Am. Chem. Soc.* **2010**, *132*, 16432–16441.

(39) Dordelmann, G.; Pfeiffer, H.; Birkner, A.; Schatzschneider, U. *Inorg. Chem.* **2011**, *50*, 4362–4367.

(40) Nakazawa, J.; Smith, B. J.; Stack, T. D. P. *J. Am. Chem. Soc.* **2012**, *134*, 2750–2759.

(41) Pulst, M.; Samiullah, M. H.; Baumeister, U.; Prehm, M.; Balko, J.; Thurn-Albrecht, T.; Busse, K.; Golitsyn, Y.; Reichert, D.; Kressler, J. *Macromolecules* **2016**, *49*, 6609–6620.

(42) Tejero, R.; Arbe, A.; Fernandez-Garcia, M.; Lopez, D. *Macromolecules* **2015**, *48*, 7180–7193.

(43) Qiu, X. P.; Tanaka, F.; Winnik, F. M., *Macromolecules* **2007**, *40*, 7069–7071.

(44) Martinez-Triana, Y. M.; Whelan, R.; Finn, M. G.; Diaz, D. D. *Macromol.*

Chem. Phys. **2017**, *218*, 1600579.

(45) Wu, P.; Feldman, A. K.; Nugent, A. K.; Hawker, C. J.; Scheel, A.; Voit, B.; Pyun, J.; Frechet, J. M. J.; Sharpless, K. B.; Fokin, V. V. *Angew. Chem. Int. Ed.* **2004**, *43*, 3928–3932.

(46) Carlmark, A.; Hawker, C. J.; Hult, A.; Malkoch, M. *Chem. Soc. Rev.* **2009**, *38*, 352–362.

(47) Wu, J. H.; Liu, W. M.; Han, H. J.; Sun, R. Y.; Xie, M. R.; Liao, X. J. *Polym. Chem.* **2015**, *6*, 4801–4808.

(48) Schulze, B.; Schubert, U. S. *Chem. Soc. Rev.* **2014**, *43*, 2522–2571.

(49) Hua, Y. R.; Flood, A. H. *Chem. Soc. Rev.* **2010,** *39*, 1262–1271.

(50) Meudtner, R. M.; Hecht, S. *Macromol. Rapid Commun.* **2008**, *29* 347–351.

(51) Mishra, V.; Jung, S. H.; Park, J. M.; Jeong, H. M.; Lee, H. I. *Macromol. Rapid Commun.* **2014**, *35*, 442–446.

(52) Jung, S. H.; Ryu, J.; Sohn, D.; Lee, H. I. *Polym. Chem.* **2012**, *3*, 1002–1006.

(53) Hu, H. Y.; Dong, T. D.; Sui, Y. Q.; Li, N. W.; Ueda, M.; Wang, L. J.; Zhang, X. *J. Mater. Chem. A* **2018**, *6*, 3560–3570.

(54) Xu, Q. L.; Lee, K. M.; Wang, F.; Yoon, J. *J. Mater. Chem.* **2011**, *21*, 15214–15217.

(55) Pretzel, D.; Sandmann, B.; Hartlieb, M.; Vitz, J.; Holzer, S.; Fritz, N.; Moszner, N.; Schubert, U. S. *J. Polym. Sci. Part A: Poly. Chem.* **2015,** *53*, 1843–1847.

(56) Sandmann, B.; Happ, B.; Kupfer, S.; Schacher, F. H.; Hager, M. D.; Schubert, U. S. *Macromol. Rapid Commun.* 2015, 36, 604–609.

(57) Song, H. B.; Baranek, A.; Worrell, B. T.; Cook, W. D.; Bowman, C. N. *Adv. Funct. Mater.* **2018**, *28*.

(58) Elloumi, A. K.; Miladi, I. A.; Serghei, A.; Taton, D.; Aissou, K.; Ben Romdhane, H.; Drockenmuller, E. *Macromolecules* **2018**, *51*, 5820–5830.

(59) Hashidzume, A.; Nakamura, T.; Sato, T. *Polymer* **2013,** *54*, 3448–3451.

(60) Noshay, A.; McGrath, J. E. *Block copolymers: overview and critical survey*. Elsevier, 2013.

(61) Mai, Y. Y.; Eisenberg, A. *Chem. Soc. Rev.* **2012**, *41*, 5969–5985.

(62) Letchford, K.; Burt, H. *Eur. J. Pharm. Biopharm.* **2007**, *65*, 259–269.

(63) Sary, N.; Richard, F.; Brochon, C.; Leclerc, N.; Leveque, P.; Audinot, J. N.; Berson, S.; Heiser, T.; Hadziioannou, G.; Mezzenga, R. *Adv. Mater.* **2010**, *22*, 763–768.

Chapter 2

Synthesis of New Diblock Copolymers of Poly(ethylene glycol) and Dense 1,2,3-Triazole Blocks: Self-Association Behavior and Thermoresponsive Property in Water

2-1. Introduction

Since the appearance of stimuli-responsive polymeric materials, thermoresponsive block copolymers are currently a center of active researches.[1-3] These copolymers, which are able to self-organize depending on temperature into a variety of aggregates,[4,5] e.g., spherical and cylindrical micelles, and vesicles, give rise to structures as "smart" carriers and nanoreactors that have a broad range of application, including drug delivery, encapsulation, catalysis, metal nanoparticle, and in vivo imaging.[6–19]

To date, poly(*N*-isopropylacrylamide) and poly(ethylene glycol) (PEG) or oligo(ethylene glycol) (OEG) are the most widely used polymers to build thermoresponsive block copolymers, especially the latter two due to their combination of lower critical solution temperature (LCST) behavior and biocompatibility.[20-23] It is well-known that the self-assembling properties and applications of block copolymer are tailored by many factors, including chemical

structure, composition, molecular weight of each block, and architecture.[24-27] The combination of different types of polymers with those thermoresponsive polymers to develop new block copolymers is an interesting challenge to enhance the application possibilities and diversity in polymer science.[28-33]

As demonstrated before, 1,2,3-triazole is an interesting nitrogen-rich aromatic heterocycle.[34–36] It can offer diverse noncovalent interactions, e.g., hydrogen bonding with protic compounds, coordination bonding with metal ions, π–π stacking, and dipole–dipole interaction.[37-41] This group is interested in functional polymers based on dense 1,2,3-triazole rings. Recently, Hashidzume et al. have prepared oligomers composed of dense 1,2,3-triazole moieties in the backbone (Scheme 1-2 in Chapter 1). The oligomer chains are strongly interacted with each other. It is believed that utilizing the dense 1,2,3-triazole block, new types of associative block copolymers can be developed.

Herein, the author has chosen well soluble and thermoresponsive PEG as one block, and synthesized a series of diblock copolymers, poly(ethylene glycol)-*b*-poly(3-azido-1-propyne) (EG*m*-*b*-AP*n*) and poly(ethylene glycol)-*b*-poly(3-azido-1-butyne) (EG*m*-*b*-AB*n*), where *m* and *n* denote the degrees of polymerization of PEG and dense 1,2,3-triazole blocks, respectively. The block copolymer samples obtained are well soluble in water. Their association behavior and thermoresponsive properties in aqueous solution are investigated by

several characterization techniques. These characterization data indicate that the dense 1,2,3-triazole block acts as hydrophobe in water, which promoted the block copolymers to self-assemble into various nanostructures although 1,2,3-triazole ring is a highly polar functional group. The influence of the relative block length and composition of triazole-based block, concentration on self-association behavior as well as the cloud point temperatures are discussed.

2-2. Materials and Methods

Materials. 3-Bromo-1-propyne (BrP), 3-bromo-1-butyne (BrB), sodium azide (NaN_3), sodium (+)-ascorbate (NaAsc), and copper(II) sulfate pentahydrate ($CuSO_4$•$5H_2O$), (≥ 99.9%) were purchased from FUJIFILM Wako Pure Chemical Co. (Osaka, Japan). Poly(ethylene glycol) (PEG) monomethyl ether (EG*m*, M_n = 750 (PDI = 1.15) and 2000 (PDI = 1.30), where *m* is the degree of polymerization (DP) of PEG) was purchased from Sigma-Aldrich (St. Louis, MO). Solvents, i.e., acetone, toluene, dichloromethane, diethyl ether, and *N*,*N*-dimethylformamide (DMF), were purchased from FUJIFILM Wako Pure Chemical Co. Water was purified by a Millipore Milli-Q system. Other reagents were used without further purification.

Measurements. ^{1}H NMR spectra were recorded on a JEOL JNM ECA500 spectrometer using tetramethylsilane or the residual solvent signal as an internal

standard in $CDCl_3$ or dimethyl sulfoxide-d_6 (DMSO-d_6). Size exclusion chromatography (SEC) measurements were carried out at 40 °C on a TOSOH HLC-8320GPC equipped with a TOSOH TSKgel SuperAWM-H column, using dimethyl sulfoxide (DMSO) containing 10 mM LiBr as eluent at a flow rate of 0.4 mL min^{-1}. Molecular weights were calibrated with PEG and poly(ethylene oxide) (PEO) standards (Scientific Polymer Products, Inc. (Ontario, NY)). All the SEC samples were passed through a 0.50 μm DISMIC JP050AN membrane filter (ADVANTEC (Tokyo, Japan)) just prior to measurements. Static and dynamic light scattering (SLS and DLS, respectively) measurements were conducted using an ALV/SLS/DLS-5000 light scattering goniometer with vertically polarized light of 532 nm. The light scattering system was calibrated using toluene as reference. Specific refractive index increments ($\partial n/\partial c$) were measured for aqueous polymer solutions at 25 °C using a Shimadzu modified Schulz-Cantow type differential refractometer with 436, 488, and 546 nm light. Interpolating of the $\partial n/\partial c$ values at 436, 488, and 546 nm, the values of $\partial n/\partial c$ at 532 nm at 25 °C were determined. Transmission electron microscopy (TEM) images were recorded by a JEOL JEM-2100 transmission electron microscope at an acceleration voltage of 120 kV. TEM specimens were prepared by dropping a 5.0 g L^{-1} aqueous solution of EG18-*b*-AP10 or EG45-*b*-AP14 onto a carbon-coated copper grid followed by drying in air. The transmittances of aqueous polymer solutions were measured at 650 nm

using a JASCO V500 UV−visible spectrometer equipped with a Peltier-type thermostatic cell holder, model ETC-505. The heating and cooling rates were fixed at 1.0 °C min^{-1}.

Preparation of Monopropargyl-Terminated EGm (EGm-P). A typical procedure for preparation of EG*m*-P is described below (Scheme 2-1).

EG18 (11.25 g, 15.0 mmol) was added in toluene (50 mL) with stirring at room temperature for 30 min. Then NaOH (2.60 g, 65.0 mmol) and BrP (1.5 mL, 20.0 mmol) were added. After stirring for 4 h, BrP (1.5 mL, 20.0 mmol) and NaOH (2.60 g, 65.0 mmol) were further added to the reaction mixture with continuous stirring for 26 h. After the colorless precipitate was removed by filtration, the solvent was also removed under reduced pressure. The residue was dissolved in saturated NaCl (100 mL). Then the product was extracted from the aqueous solution with dichloromethane (3 × 50 mL). The organic phases were combined. The combined organic layer was washed with saturated NaCl (2 × 100 mL). After drying the organic phase with anhydrous $MgSO_4$, dichloromethane was evaporated under reduced pressure to obtain a crude product. Finally, the product was purified by reprecipitation twice using dichloromethane and hexane. After drying under vacuum at 45 °C for 24 h, the product EG18-P was recovered as pale yellow gel (10.1 g, 85.7% yield). Dichloromethane must be removed completely from EG18-P because it may react with NaN_3 to form

diazidomethane in the next reaction. ^{1}H NMR (500 MHz, $CDCl_3$) δ (ppm): 4.23–4.17 (br, 2H), 3.75–3.50 (br, 4H), 3.38–3.35 (br, 3H), 2.45–2.40 (br, H).

Preparation of Diblock Copolymers EGm-b-APn and EGm-b-ABn. A typical procedure of preparation of EG*m*-*b*-AP*n*, where *n* is DP of AP block, is described below (Scheme 2-1).

EG18-P (1.88 g, 2.5 mmol) was dissolved in DMF (3 mL). $CuSO_4$•$5H_2O$ (0.0625 g, 0.25 mmol) and NaAsc (0.0600 g, 0.3 mmol) were added to a 100 mL flask under a nitrogen atmosphere. The mixture was stirred for 5 min. Then, NaN_3 (1.95 g, 30 mmol) and BrP (2.8 mL, 25 mmol, 80 wt% in toluene) were added to the reaction mixture. The reaction mixture was warmed with an oil bath thermostated at 80 °C with stirring. After 72 h, the reaction mixture was poured into DMF (50 mL). The precipitate was removed by filtration. The solution was passed through a neutral Al_2O_3 column. The volatile fraction was removed under reduced pressure and then the residue obtained was dissolved in water (100 mL). The precipitate formed was removed from the solution by centrifugation. Water was removed under reduced pressure. The product obtained, EG18-*b*-AP*m*, was then extracted with dichloromethane (3 × 50 mL) to remove inorganic salt. EG18-*b*-AP*m* was recovered as brown solid after drying at 80 °C under vacuum (2.09 g, 53.6% yield). ^{1}H NMR (500 MHz, DMSO-d_6) δ (ppm): 8.49–

7.54 (br, H), 6.16–5.45 (br, 2H), 4.75–4.35 (br, 2H), 3.75–3.31 (br, 4H), 3.30–3.25 (br, 3H).

Diblock copolymer EG18-*b*-AB7 was prepared in the same method by using the corresponding monomer precursor BrB.

Analysis of Light Scattering Data.[42-45] The intensity autocorrelation function $g^{(2)}(t)$ obtained by dynamic light scattering was analyzed by a CONTIN program to estimate the spectrum $A(\tau, k)$ of the relaxation time τ in the logarithmic scale at each scattering angle or the magnitude of the scattering vector k. In the case where $A(\tau, k)$ was bimodal, the sample contains two scattering components with fast and slow relaxation times. Using the $A(\tau, k)$ data, R_θ obtained from static light scattering measurement was divided into the fast- and slow-relaxation components according to the following equations

$$R_{\theta,\text{fast}} = R_\theta \sum_{\tau \in \text{fast}} A(\tau,k) \quad , \quad R_{\theta,\text{slow}} = R_\theta \sum_{\tau \in \text{slow}} A(\tau,k) \tag{1}$$

where $A(\tau, k)$ is assumed to be normalized.

When the solution is dilute enough, $R_{\theta,i}$ (i = fast, slow) can be written as

$$\lim_{\theta \to 0} \left(\frac{Kc}{R_{\theta,i}} \right)^{1/2} = \frac{1}{\left(w_i M_{\text{w},i} \right)^{1/2}} + A_{2,i} \left(w_i M_{\text{w},i} \right)^{1/2} c + \cdots \tag{2}$$

and

$$\lim_{c\to 0}\left(\frac{Kc}{R_{\theta,i}}\right)^{1/2} = \frac{1}{\left(w_i M_{\mathrm{w},i}\right)^{1/2}}\left(1+\frac{1}{6}\langle S^2\rangle_{\mathrm{z},i}k^2+\cdots\right) \tag{3}$$

where K is the optical constant, c is the total polymer mass concentration, and w_i, $M_{\mathrm{w},i}$, $\langle S^2\rangle_{z,i}$, and $A_{2,i}$ are the weight fraction (in the total polymer), weight average molar mass, z-average mean square radius of gyration, and second virial coefficient of the component i, respectively. If $w_{\mathrm{slow}} << w_{\mathrm{fast}}$, $A_{2,\mathrm{fast}}$ is equal to the second virial coefficient between fast-relaxation components, while $A_{2,\mathrm{slow}}$ approximately equals to the one between the fast- and slow-relaxation components multiplied by $w_{\mathrm{fast}}M_{\mathrm{w,fast}}/w_{\mathrm{slow}}M_{\mathrm{w,slow}}$.

From bimodal $A(\tau, k)$, the first cumulants of the fast component Γ_{fast} and the slow component Γ_{slow} were estimated by

$$\Gamma_{\mathrm{fast}} = \sum_{\tau\in\mathrm{fast}}\tau^{-1}A(\tau,k)\Big/\sum_{\tau\in\mathrm{fast}}A(\tau,k), \quad \Gamma_{\mathrm{slow}} = \sum_{\tau\in\mathrm{slow}}\tau^{-1}A(\tau,k)\Big/\sum_{\tau\in\mathrm{slow}}A(\tau,k) \tag{4}$$

The diffusion coefficient $D_{0,i}$ and the hydrodynamic radius $R_{\mathrm{H},i}$ of the component i (i = fast, slow) were determined by

$$\lim_{k,c\to 0}\Gamma_i\Big/k^2 = D_{0,i}, \quad R_{\mathrm{H},i} = k_{\mathrm{B}}T\Big/6\pi\eta_{\mathrm{solv}}D_{0,i} \tag{S5}$$

where $k_{\mathrm{B}}T$ is the Boltzmann constant multiplied by the absolute temperature, and η_{solv} is the solvent viscosity.

Scheme 2-1. Synthetic Route of EG*m*-*b*-AP*n* and EG*m*-*b*-AB*n* Diblock Copolymers

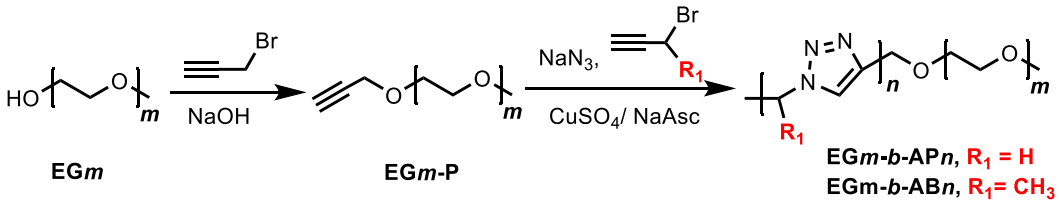

2-3. Results and Discussion

To prepare EG*m*-*b*-AP*n* and EG*m*-*b*-AB*n*, PEG monomethyl ether (EG*m*) was initially modified with a propargyl group by reaction with BrP in the presence of NaOH to obtain EG*m*-P.[46] In the presence of the EG*m*-P obtained, CuAAC polymerization of AP or AB was carried out in DMF at 80 °C using $CuSO_4$•$5H_2O$/NaAsc pair as a Cu(I) catalyst. Since it is likely that AP and AB are highly explosive, BrP or BrB was used as the monomer precursor, respectively, and converted to the monomer in situ by reaction with NaN_3 (Scheme 1). In this study, two EG*m* samples of different molecular weights (M_n = 750 and 2000) were employed. From the ^{1}H NMR spectra in Figure 2-1, *m* values of two EG*m*-P samples were determined to be ca. 18 and 45, which agreed with the information given by the supplier. Using the ratio of area intensities of signals at 2.4 and 3.4 ppm, the degrees of substitution were determined to be ca. 97 and 88 % for EG18-P and EG45-P, respectively.

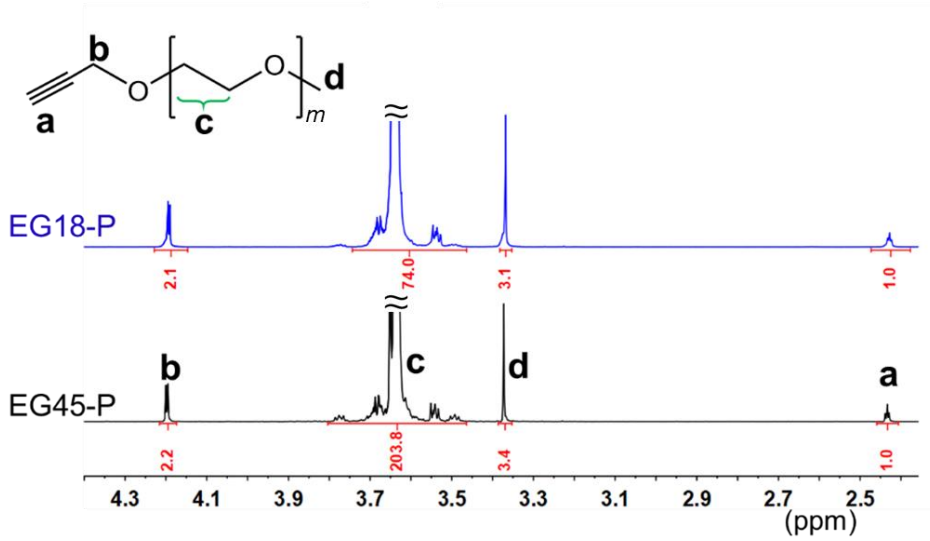

Figure 2-1. ^{1}H NMR spectra of EG*m*-P in $CDCl_3$ (500 MHz, 25 °C).

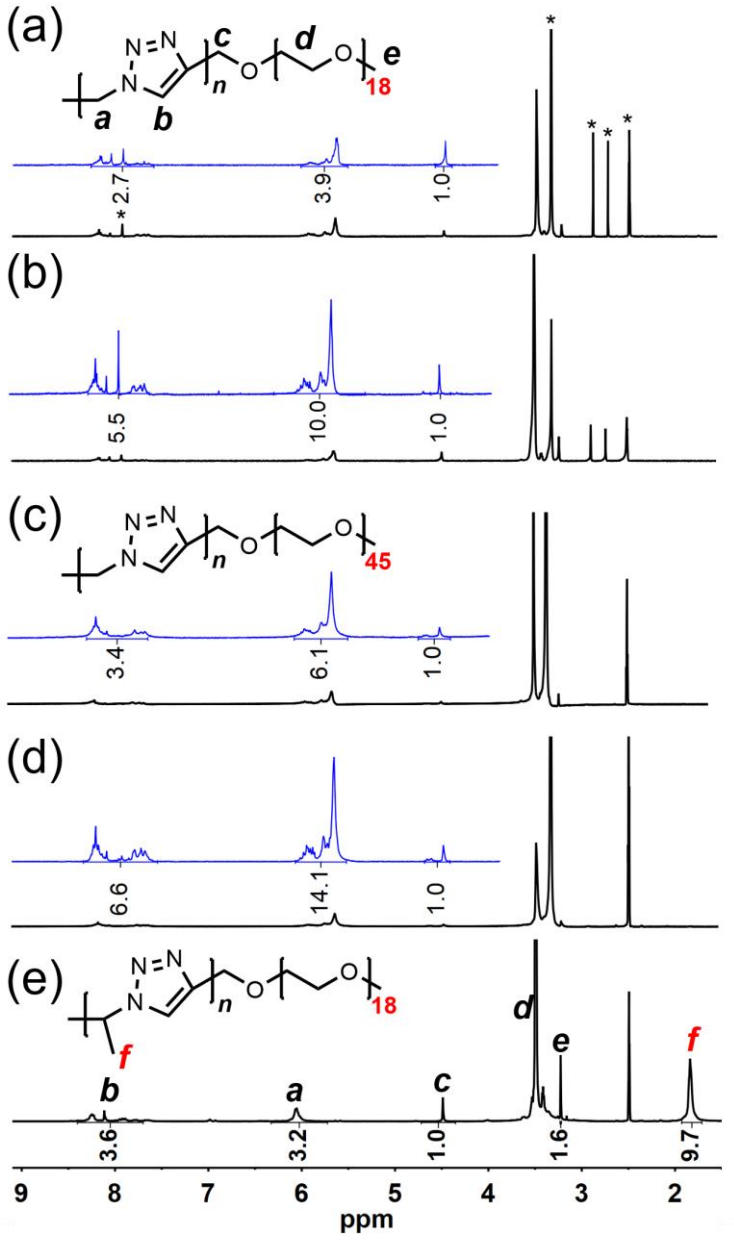

Figure 2-2. ^{1}H NMR spectra for EG*m*-*b*-AP*n* and EG18-*b*-AB7 diblock copolymers in DMSO-d_6 (500 MHz, 25 °C), respectively. Asterisks denote signals due to the residual solvents.

Figure 2-2 presents the ^{1}H NMR spectra of diblock copolymers prepared. The spectra for EG*m*-*b*-AP*n* and EG18-*b*-AB*n* do not indicate any signals ascribable to the ethynyl and methylene protons of EG*m*-P at 2.4 and 4.2 ppm in Figure 2-1, whereas new signals assignable to the methylene protons neighboring the 1,2,3-triazole ring at 4.5 ppm and broad signals assignable to the proton in 1,2,3-triazole ring and the methylene protons between 1,2,3-triazole rings at 7.5 – 8.5 and 5.5 – 6.3 ppm were observed, indicating that all the propargyl functional groups in EG*m*-P reacted with monomers. Figure 2-2c presents the ^{1}H NMR spectrum for EG18-*b*-AB*n*, proton signals of the methylene, methine, and 1,2,3-triazole protons, as well as the new signal ascribed to the methyl side chain in AB*n* block at ca. 1.9 ppm were observed. On the basis of the ratio of area intensities, the *n* values for EG18-*b*-AP*n* were evaluated to be ca. 4 and 10, and those for EG45-*b*-AP*n* to be ca. 6 and 14, and for AB*n* block to be ca. 7. EG*m*-P and corresponding diblock copolymers were also characterized by SEC (Figure 2-3) using DMSO as eluent, which is a good solvent for diblock copolymers from Table 3-2 and Figure 3-2 in Chapter 3. In comparison to EG*m*-P, all the SEC traces of block copolymers shifted toward a shorter eluent time, indicative of an increased molecular weight. Moreover, this figure shows unimodal molecular weight distributions for EG*m*-*b*-AP*n* and EG18-*b*-AB7 samples, indicating the successful preparation and purification. (The polymerization mixture should contain PAP or PAB

homopolymer.) These ^{1}H NMR and SEC data are indicative of successful preparation of EG*m*-*b*-AP*n* and EG18-*b*-AB7 samples. The basic characteristics of the copolymer samples are summarized in Table 2-1. It should be noted that with the increase of AP*n* block length, the control over the polymerization and solubility in DMSO decreased. A broader polydispersity and deviation of M_n determined by SEC and NMR of EG18-*b*-AP10 were thus observed.

Table 2-1. Basic Characteristics of Diblock Copolymers in This Study

polymer code [a]	molar feed ratio EG*m* : precursor [b]	*m*/*n* [a]	$M_{n,NMR}$ [c] /10^3	$M_{n,SEC}$ [d] /10^{-3}	M_w/M_n [d]
EG18-*b*-AP4	1 : 3	4.5	1.1	1.5	1.3
EG18-*b*-AP10	1 : 10	1.8	1.6	3.0	2.0
EG45-*b*-AP6	1 : 10	7.5	2.5	2.7	1.4
EG45-*b*-AP14	1 : 20	3.2	3.1	2.7	4.2
EG18-*b*-AB7	1 : 5	2.6	1.4	1.5	1.2

a. DP values were determined by ^{1}H NMR spectroscopy. *b*. BrP and BrB were used as the monomer precursor for CuAAC polymerization. *c*. Calculated from the DP data determined by ^{1}H NMR spectroscopy. *d*. Determined by SEC using DMSO as eluent. Molecular weights were calibrated with PEG standard samples.

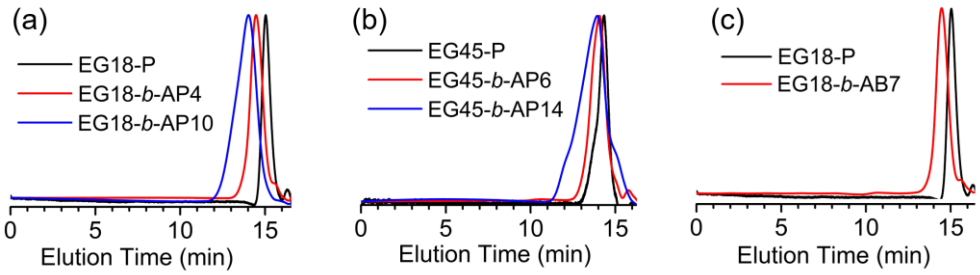

Figure 2-3. SEC data for EG18-P, EG18-*b*-AP4, and EG18-*b*-AP10 (a); EG45-P, EG45-*b*-AP6, and EG45-*b*-AP14 (b); EG18-P and EG18-*b*-AB7 (c).

All the EG*m*-*b*-AP*n* and EG18-*b*-AB7 diblock copolymer samples were well soluble in water, although AP and AB oligomers are insoluble in water. The self-association behavior has been thus studied in water by ^{1}H NMR, SLS, DLS, and TEM.

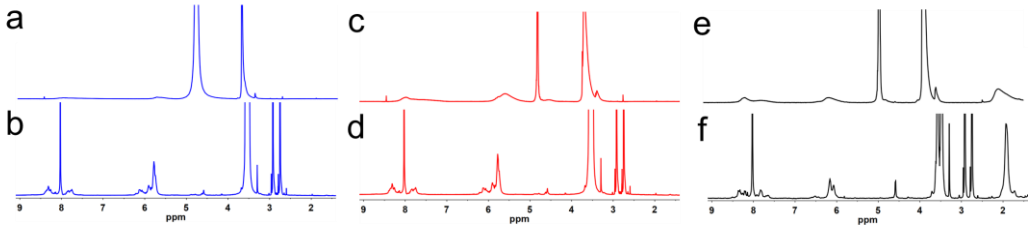

Figure 2-4. ^{1}H NMR spectra of EG18-*b*-AP10 (a, b), EG45-*b*-AP14 (c, d), and EG18-*b*-AB7 (e, f) at 5.0 g L^{-1} in D_2O (a, c, e) and DMF-d_7 (b, d, f), respectively.

Figure 2-4 compares ^{1}H NMR spectra measured for EG18-*b*-AP10, EG45-*b*-AP14, and EG18-*b*-AB7 in DMF-d_7 and D_2O at 5.0 g L^{-1}. As can be seen in Figures 2-4b, 4d, and 4f, the ^{1}H NMR spectra in DMF-d_7 indicate rather sharp signals ascribable to the PEG and dense 1,2,3-triazole blocks, indicating that all the EG18-*b*-AP10, EG45-*b*-AP14, and EG18-*b*-AB7 chains are dispersed molecularly in this medium. While the spectra in D_2O exhibit markedly weak and broad signals due to the dense 1,2,3-triazole blocks although signals due to the PEG blocks are still sharp (Figures 2-4a, 4c, and 4e). These observations indicate that EG18-*b*-AP10, EG45-*b*-AP14, and EG18-*b*-AB7 chains form aggregates in D_2O, in which the mobility of dense 1,2,3-triazole blocks is highly restricted. It is thus likely that the aggregates are formed through dipole–dipole interaction of the dense 1,2,3-triazole blocks.

Figure 2-5 displays typical examples of DLS data measured for 5.0 g L^{-1} aqueous solutions of EG*m*-*b*-AP*n* and EG18-*b*-AB7 at 25 °C. Here, the abscissa is the delay time (t) or relaxation time (τ) multiplied by $(k_BT/6\pi\eta_S)k^2$, i.e., $t(k_BT/6\pi\eta_S)k^2$ or $\tau(k_BT/6\pi\eta_S)k^2$, which corresponds to the apparent hydrodynamic radius ($R_{H,app}$). The DLS data for shorter diblock copolymers, EG18-*b*-AP4, EG18-*b*-AP10, and EG18-*b*-AB7, show unimodal size distributions (Figures 2-5a, 5b, and 5e), whereas those for the longer diblock copolymers, EG45-*b*-AP6 and EG45-*b*-AP14, exhibit bimodal distributions (Figures 2-5c and 5d). It should be

noted here that all the DLS data include a relaxation component with $R_{H,app}$ > 10 nm, indicative of the formation of aggregates because the end-to-end distance of stretched chain for EG18-*b*-AP10 was calculated to be only ca. 11.0 nm.

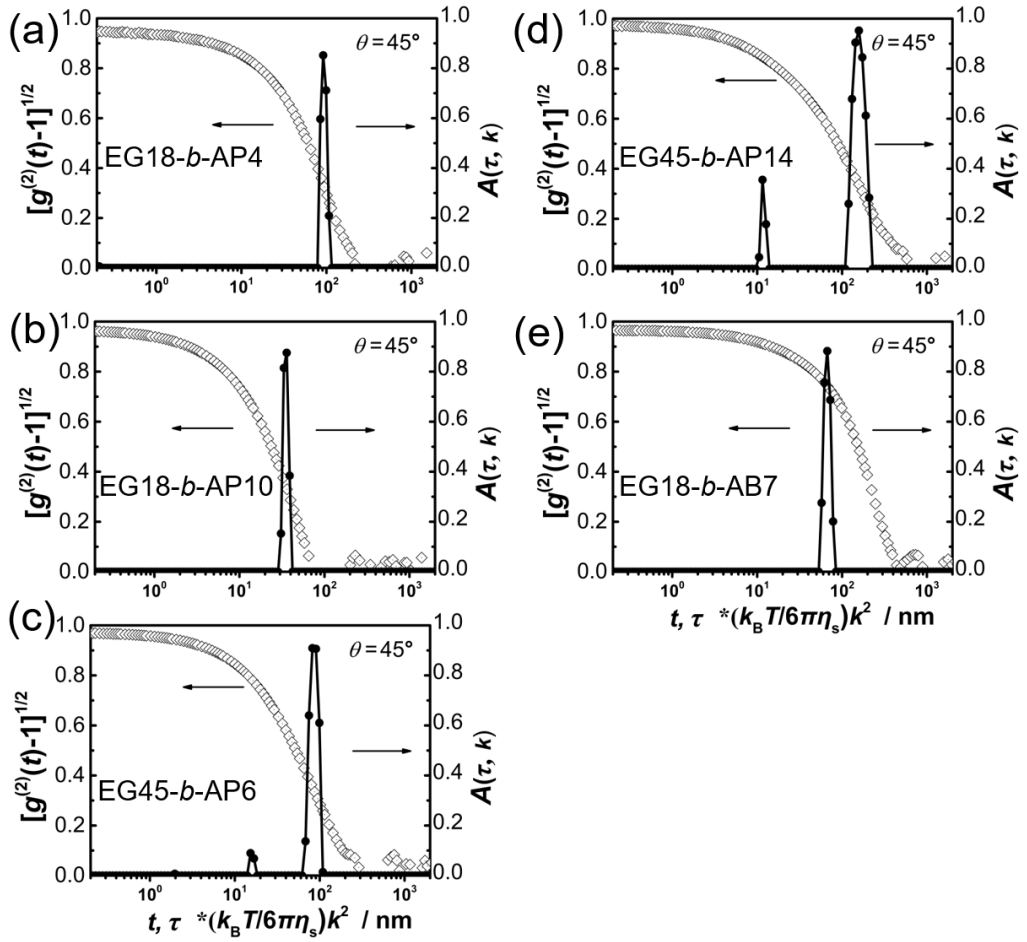

Figure 2-5. DLS data for 5.0 g L^{-1} aqueous solutions of EG18-*b*-AP4 (a), EG18-*b*-AP10 (b), EG45-*b*-AP6 (c), EG45-*b*-AP14 (d), and EG18-*b*-AB7 diblock copolymers (e).

To investigate detail structure of aggregates, SLS and DLS measurements at different scattering angles and concentrations were carried out. In the cases of bimodal distribution, the SLS data were divided into the fast and slow modes using the DLS data (see experimental section).[42-45] It should be noted here that EG18-b-AB7 show unimodal size distribution (Figure 2-5e), while bimodal size distributions were observed at concentration less than 5.0 g L^{-1}. The scattering angular dependencies of $(Kc/R_\theta)^{1/2}$ and concentration dependencies of $(Kc/R_0)^{1/2}$ (obtained by extrapolating $(Kc/R_\theta)^{1/2}$ to scattering angle θ = 0º) and Γ/k^2 are reasonable as shown in Figures 2-6 and 2-7. Analyzing these data for the fast and slow modes separately, the hydrodynamic radius (R_H), molar masses of the fast mode ($M_{w,fast}$) and radii of gyration of the fast and slow modes ($\langle S^2\rangle_{z,fast}^{1/2}$ and $\langle S^2\rangle_{z,slow}^{1/2}$, respectively) were evaluated. The data evaluated for the fast and slow modes are summarized in Tables 2-2 and 2-3, respectively. Here, the $\langle S^2\rangle_{z,fast}^{1/2}$ values were too small for EG18-*b*-AP10 and EG18-*b*-AB7 to be determined. The specific structure of the fast mode formed by EG18-*b*-AP10 and EG18-*b*-AB7 cannot be determined from these data. Further measurements, e.g., SAXS are helpful for the structure analysis. For the fast modes, $M_{w,fast}$ ranges $(2.6 – 15.5) \times 10^5$ and thus the aggregation number (N_{agg}), i.e., the number of polymer chains per aggregate, ranges $(1.76 – 6.24) \times 10^2$. The ρ (= $\langle S^2\rangle_{z,fast}^{1/2}/R_{H,fast}$) values for EG45-*b*-AP6 and EG45-*b*-AP14 (0.735 and 0.817,

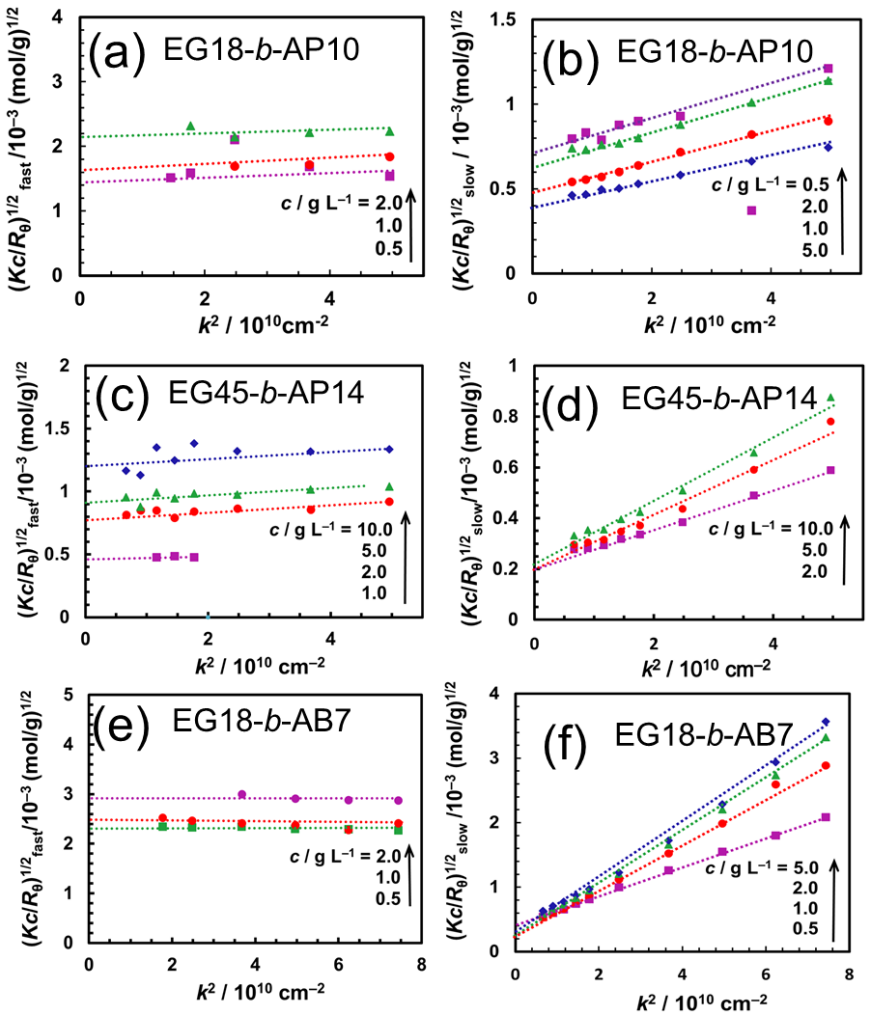

Figure 2-6. Angular dependencies of fast- (a, c, e) and slow-relaxation components (b, d, f) of $(Kc/R_\theta)^{1/2}$ for aqueous solutions of EG18-*b*-AP10 (a, b), EG45-*b*-AP14 (c, d), and EG18-*b*-AB7 (e, f) at different concentrations.

respectively) are indicative of the formation of spherical micelles in aqueous solution. Using these data, the surface areas ($A_{PEG} = 4\pi R_H^2/N_{agg}$) occupied by a

PEG block in the spherical micelles were calculated to be 23.3 and 4.7 nm^2 for EG45-*b*-AP6 and EG45-*b*-AP14, respectively. These A_{PEG} values indicate that EG45-*b*-AP14 chains are packed more densely in the spherical micelle than EG45-*b*-AP6 chains because the longer AP14 blocks interact more strongly with each other than do the shorter AP6 blocks. On the basis of the ρ values for slow component in Table 3, it is likely that EG18-*b*-AP4 and EG18-*b*-AP10 chains form vesicles (ρ = 1.01 and 1.02), whereas EG18-*b*-AB7 chains form rodlike micelles (ρ = 2.31). It was not possible to determine $M_{w,slow}$, because the weight fraction of slow mode is usually too small and it is not possible to evaluate the concentration of slow mode.

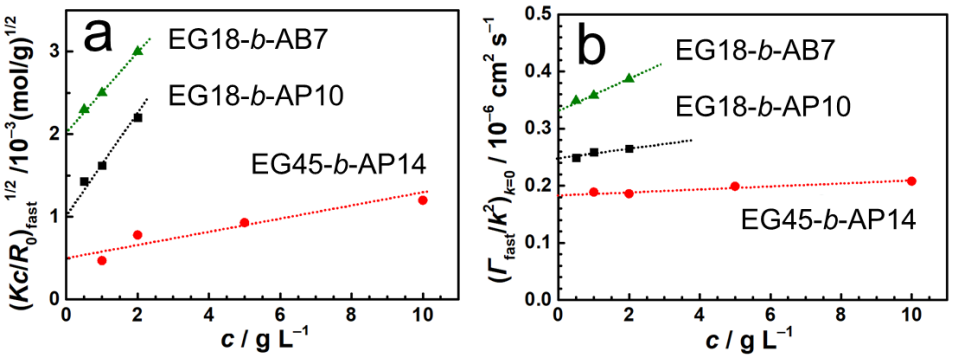

Figure 2-7. Concentration dependencies of $(Kc/R_0)_{fast}^{1/2}$ (a) and $(\Gamma_{fast}/k^2)_{k=0}$ (b) for aqueous solutions of diblock copolymers.

Table 2-2. Structural Parameters of the Fast Relaxation Component in Water

polymer code	$M_{w,fast}$ / 10^5	$\langle S^2 \rangle_{z,fast}^{1/2}$/nm	N_{agg} / 10^2	$R_{H,fast}$ / nm	ρ_{fast}
EG18-*b*-AP10	4.38	–	2.74	9.9	–
EG45-*b*-AP6	15.5	25	6.24	34	0.735
EG45-*b*-AP14	14.3	10.7	4.61	13.1	0.817
EG18-*b*-AB7	2.57	–	1.76	7.0	–

Table 2-3. Structural Parameters of the Slow Relaxation Component in Water

polymer code	$\langle S^2 \rangle_{z,slow}^{1/2}$ / nm	$R_{H,slow}$ / nm	ρ_{slow}
EG18-*b*-AP4	93	92	1.01
EG18-*b*-AP10	42	41	1.02
EG45-*b*-AP6	94	95	0.99
EG45-*b*-AP14	107	148	0.72
EG18-*b*-AB7	125	54	2.31

The aggregates formed from EG18-*b*-AP10 and EG45-*b*-AP14 were also characterized by TEM observations, as shown in Figure 2-8. TEM specimens were prepared by dropping a 5.0 g L^{-1} aqueous polymer solutions onto a carbon-coated copper grid followed by drying in air. The TEM images display that EG18-*b*-AP10 forms spherical objects of 90 – 130 nm in diameter (Figure 2-8a).

It is noteworthy that Figure 2-8a contains hollow objects, as can be seen in the inset. This observation is indicative of the formation of vesicles from EG18-*b*-AP10, in which the shell is ca. 50 nm thick. On the other hand, EG45-*b*-AP14 forms dominantly smaller spherical objects of 20 – 30 nm in diameter as well as larger aggregates of 100 – 300 nm in diameter as minor components (Figure 2-8b). These observations agree well with the data obtained by SLS and DLS measurements (Tables 2-2 and 2-3).

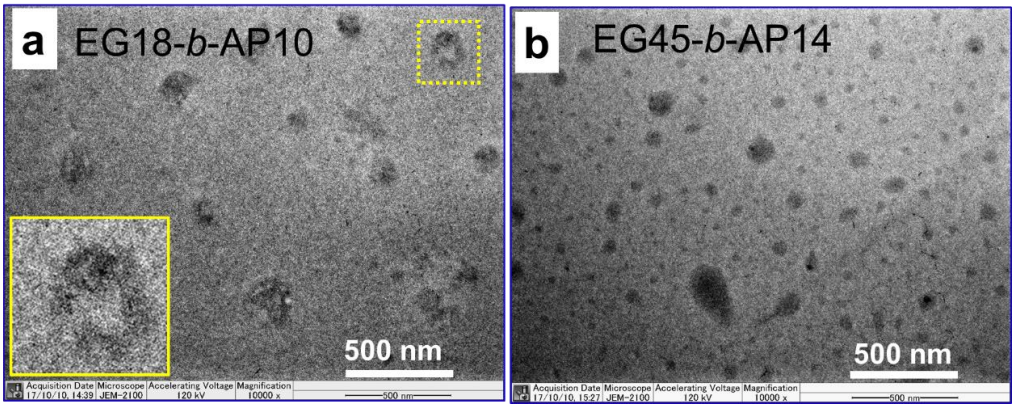

Figure 2-8. TEM images for aggregates formed from EG18-*b*-AP10 (a) and EG45-*b*-AP14 (b). The specimens were prepared by dropping a 5.0 g L^{-1} aqueous polymer solution onto a carbon-coated copper grid and then drying in air.

It is well-known that aqueous solutions of PEG and OEG undergo phase separation at higher temperatures, i.e., LCST-type phase separation.[46] Currently, most research used OEG in side chains to develop thermoresponsive polymers

since the LCST of PEG is typically higher than 100 °C. But aqueous solutions of EG18-b-AP10, EG45-b-AP14, and EG18-b-AB7 copolymers exhibited reversible thermal phase transitions behavior with a broad variable temperature range from 42 – 80 °C, depending on the copolymer composition, structure, and concentration as shown in Figure 2-9a. These temperatures are far below the cloud point of the PEG precursor, i.e. 170 – 180 °C for EG45 (M_w = 2.0 × 10^3 g mol^{-1}) and even higher for EG18. However, the aqueous solutions of EG18-*b*-AP4 and EG45-*b*-AP6 exhibited higher constant transmittances in the whole temperature range examined and did not undergo phase separation. Since these polymers of lower *n*/*m* (≤ 0.22) are hydrophilic, it is likely that the LCST-type phase separation requires *n*/*m* higher than a certain critical value. As can be seen in Figure 2-9a, a 5.0 g L^{-1} aqueous solution of EG18-*b*-AP10 shows lower transmittances (ca. 60%) even in the lower temperature regime, indicative of the formation of larger aggregates, i.e., vesicles. As the temperature is increased, the transmittance abruptly decreases to 0% in a narrow temperature range of 65 – 70 °C, resulting in phase separation. As the temperature is decreased, the transmittance returns to the initial value in a slightly lower temperature range than that for the heating process. Using these transmittance data for 5.0 g L^{-1} EG18-*b*-AP10, the clouding-point temperature (T_{cloud}) in the heating process and the clearing-point temperature (T_{clear}) in the cooling process were evaluated to be 64.8 and 60.0 °C,

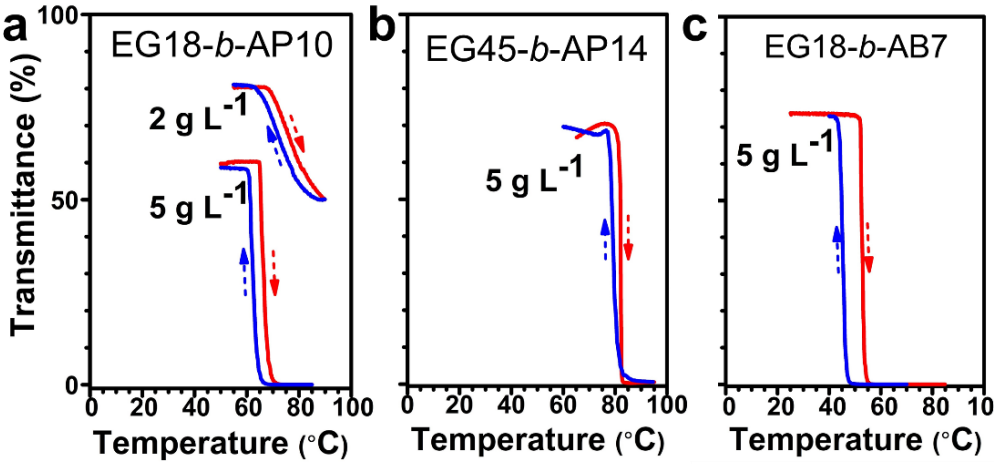

Figure 2-9. Transmittance data for aqueous solutions of EG18-*b*-AP10 (2.0 and 5.0 g L^{-1}) (a), EG45-*b*-AP14 (5.0 g L^{-1}) (b), and EG18-*b*-AB7 (5.0 g L^{-1}) (c) monitored at 650 nm with heating (red) and cooling (blue) at 0.10 °C min^{-1}.

respectively. A 2.0 g L^{-1} aqueous solution of EG18-*b*-AP10 shows higher transmittances than those for 5.0 g L^{-1} EG18-*b*-AP10, i.e., ca. 80 and 50% in the lower and higher temperature regimes, respectively, indicative of a weak concentration dependency of aggregation of the diblock polymer. However, it should be noted here that T_{cloud} (67.5 °C) and T_{clear} (63.8 °C) are only slightly higher than those at 5.0 g L^{-1}, indicating that the LCST-type phase behavior is dependent predominantly on the ratio of block lengths, i.e., n/m. Similarly, values of T_{cloud} and T_{clear} were also evaluated for aqueous solutions of EG45-*b*-

AP14 and EG18-*b*-AP7 using the data in Figures 2-9b and 2-9c. Table 2-4 summarizes the T_{cloud} and T_{clear} values determined. T_{cloud} and T_{clear} for EG18-*b*-AP10 are lower than those for EG45-*b*-AP14, and the difference between T_{cloud} and T_{clear}, i.e., the hysteresis, for EG18-*b*-AP10 is larger than that for EG45-*b*-AP14. These data indicate that EG18-*b*-AP10 is more hydrophobic than EG45-*b*-AP14, consistent with the *n*/*m* values of these diblock copolymers. T_{cloud} and T_{clear} for EG18-*b*-AP10 are higher than those for EG18-*b*-AB7, and the hysteresis for EG18-*b*-AP10 is smaller than that for EG18-*b*-AB7, indicating that EG18-*b*-AB7 is more hydrophobic than EG18-*b*-AP10. It is thus likely that the methyl substituent in AB unit makes the polymer more hydrophobic.

Table 2-4. Clouding-Point and Clearing-Point Temperatures for Aqueous Solutions of EG*m*-*b*-AP*n* and EG18-*b*-AB7

polymer code	*n*/*m*	concentration / g L^{-1}	T_{cloud} / °C	T_{clear} / °C
EG18-*b*-AP4	0.22	5.0	–	–
EG18-*b*-AP10	0.56	5.0	64.8	60.0
EG18-*b*-AP10	0.56	2.0	67.5	63.8
EG45-*b*-AP6	0.13	5.0	–	–
EG45-*b*-AP14	0.31	5.0	79.7	77.1
EG18-b-AB7	0.39	5.0	51.5	42.3

How the polymer aggregates behave at higher temperatures was investigated by ^{1}H NMR and DLS. Figure 2-10 demonstrates ^{1}H NMR spectra measured for a 5.0 g L^{-1} solution of EG18-*b*-AP10 in D_2O at varying temperatures. The broad signals due to AP10 block at ca. 5.5 and 8.0 ppm did not change significantly, whereas the signals ascribed to EG18 block at ca. 3.6 ppm became weaker at temperatures ≥ 70 °C, indicative of the restricted mobility of EG18 blocks. It is thus concluded that EG18 blocks are dehydrated and then aggregate at temperature higher than T_{cloud} (or T_{clear}). A typical example of DLS measured for 5.0 g L^{-1} EG18-*b*-AP10 at 70 °C were also carried out (not shown). A narrow unimodal size distribution at $R_{H,app}$ ~ 200 nm is detected. This observation indicates that a certain number of EG18-*b*-AP10 vesicles form a larger aggregate at 70 °C, which is a temperature slightly higher than T_{cloud}.

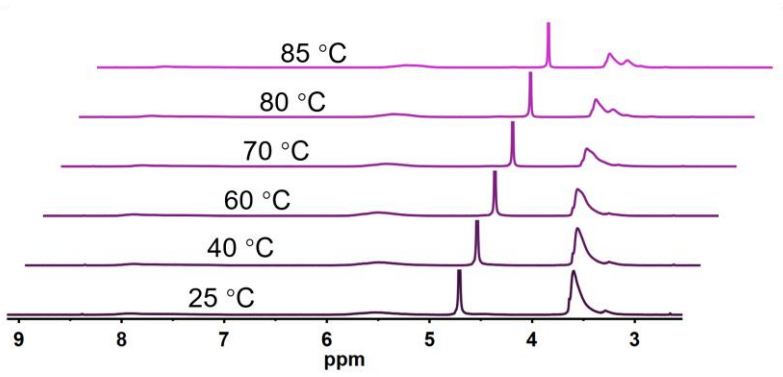

Figure 2-10. ^{1}H NMR spectra for a 5.0 g L^{-1} solution of EG18-*b*-AP10 in D_2O at varying temperatures from 25 to 85 °C.

On the basis of the characterization data described above, the association

behavior of EG18-*b*-AP10 and EG45-*b*-AP14 in water is illustrated in Scheme 2-2. These diblock copolymers form aggregates presumably through the dipole–dipole interaction of dense 1,2,3-triazole blocks; EG18-*b*-AP10 chains form vesicles, whereas EG45-*b*-AP14 chains form spherical micelles, depending on the ratio of block lengths, *n*/*m*. Both the vesicles and micelles further aggregate at higher temperatures because of dehydration of EG blocks, resulting in the LCST-type phase separation. It is thus concluded that the thermoresponsive association behavior can be controlled by adjusting the ratio of block lengths, *n*/*m*, or by attaching methyl substituents. We expect that the results presented in this study contribute to the development of new materials based on dense 1,2,3-triazole block.

Scheme 2-2. Schematic illustration of thermoresponsive self-association behavior of EG18-*b*-AP10 and EG45-*b*-AP14 in water.

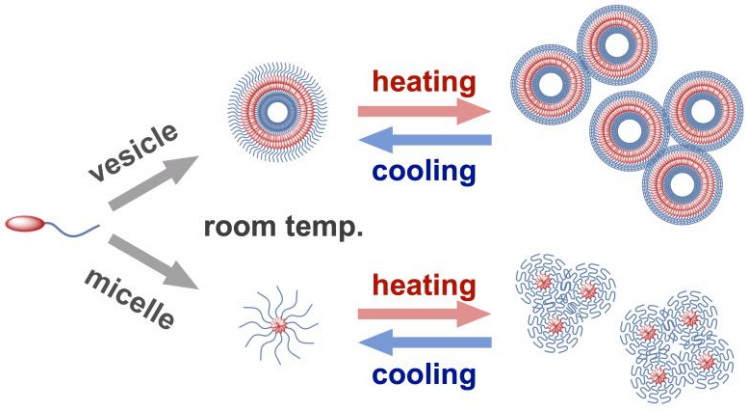

Domains formed from dense 1,2,3-triazole blocks provide locally highly polar media, which are different from hydrophobic domains formed from aliphatic or aromatic hydrocarbons. It is thus expected that aggregates of EG*m*-*b*-AP*n* and EG*m*-*b*-AB*n* capture polar molecules or metal ions, which interact with 1,2,3-trizole. Since 1,2,3-triazole block can be quarternized with alkyl halide to form a polymeric ionic liquid,[48,49] quarternized EG*m*-*b*-AP*n* and EG*m*-*b*-AB*n* may be utilized to electrochemical applications, e.g., polyelectrolyte membranes.

2-4. Conclusion

New diblock copolymers, EG*m*-*b*-AP*n* and EG18-*b*-AB7, possessing a dense 1,2,3-triazole block, were synthesized by CuAAC polymerization of AP and AB, respectively, in the presence of EG*m*-P. All the EG*m*-*b*-AP*n* and EG18-*b*-AB7 copolymer samples were well soluble in water. The self-association behavior in water was systematically studied. The dense 1,2,3-triazole blocks act as hydrophobe in water presumably through the strong dipole–dipole interaction offered by the dense 1,2,3-triazole rings, although 1,2,3-triazole rings has large dipole moment and can form hydrogen bonding. All the diblock copolymers can self-assemble into different aggregates, i.e. spherical micelles, vesicles, and cylindrical micelles even with relative short dense 1,2,3-triazole blocks, e.g. EG18-*b*-AP4 and EG45-*b*-AP6. The self-assemblies formed by EG18-b-AP10,

EG45-b-AP14, and EG18-b-AB7 underwent further aggregation and exhibited thermoresponsive properties. The thermoresponsive association behavior was controlled by the relative block length and composition of dense 1,2,3-trizole blocks. The domains formed from dense 1,2,3-triazole blocks provide highly polar media and offer diverse supramolecular interactions are highly promising as new nanoreactor or drug delivery carriers for specific applications.

References

(1) Zhu, Y.; Yang, B.; Chen, S. Prog. *Polym. Sci.* **2017**, *64*, 1–22;

(2) Mura, S.; Nicolas, J.; Couvreur, P. *Nat. Mater.* **2013**, *12*, 991−1003.

(3) Strandman, S.; Zhu, X. X. *Prog. Polym. Sci.* **2015**, *42*, 154–176.

(4) Roy, D.; Brooks, W. L. A.; Sumerlin, B. S. *Chem. Soc. Rev.* **2013**, *42*, 7214−7243

(5) Vancoillie, G.; Frank, D.; Hoogenboom, R. *Prog. Polym. Sci.* **2014**, 39, 1074−1095.

(6) Ward, M. A.; Georgiou, T. K. *Polymers* **2011**, *3*, 1215–1242.

(7) Madsen J.; Armes, S. P. *Soft Matter* **2012**, *8*, 592–605.

(8) Rösler, A.; Vandermeulen, G. W. M.; Klok, H.-A. *Adv. Drug Delivery Rev.* **2001**, *53*, 95–108.

(9) Torchilin, V. P. *Pharm. Res.* **2007**, *24*, 1–16.

(10) Adams, M. L.; Lavasanifar, A.; Kwon, G. S. *J. Pharm. Sci.* **2003**, *92*, 1343–1355.

(11) York, A. W.; Kirkland, S. E.; McCormick, C. L. *Adv. Drug Delivery Rev.* **2008**, *60*, 1018–1036.

(12) Mura, S.; Nicolas, J.; Couvreur, P. *Nat. Mater.* **2013**, *12*, 991–1003.

(13) Nardin, C.; Widmer, J.; Winterhalter, M.; Meier, W. *Eur. Phys. J. E* **2001**, *4*, 403–410.

(14) Renggli, K.; Baumann, P.; Langowska, K.; Onaca, O.; Bruns, N.; Meier, W. *Adv. Funct. Mater.* **2011**, *21*, 1241–1259.

(15) Gaitzsch, J.; Huang, X.; Voit, B. *Chem. Rev.* **2016**, *116*, 1053–1093.

(16) Bronstein, L.; Krämer, E.; Berton, B.; Burger, C.; Förster, S.; Antonietti, M. *Chem. Mater.* **1999**, *11*, 1402–1405.

(17) Mayer, A. B. R. *Polym. Adv. Technol.* **2001**, *12*, 96–106.

(18) Shin, N. H.; Lee, J. K.; Li, H.; Ha, C.-S.; Shchipunov, Y. A.; Kim, I. *J. Nanosci. Nanotechnol.* **2010**, *10*, 6948–6953.

(19) Lutz, J.-F. *J. Polym. Sci. Part A: Polym. Chem.* **2008**, *46*, 3459–3470.

(20) Rzaev, Z. M. O.; Dincer S.; Pişkin E. *Prog. Polym. Sci.* **2007**, *32*, 534–595.

(21) Roth, P. J.; Davis, T. P.; Lowe, A. B. *Macromolecules* **2012**, *45*, 3221–

3230.

(22) Bera, D.; Verdonck, L.; Glassner, M.; Madder, A.,; Hoogenboom, R.; *Macromol. Rapid Commun.* **2019**. 1800900.

(23) Cui, Q.; Wu, F.,;Wang, E. *J. Phys. Chem. B* **2011**, *115*, 5913–5922.

(24) Kelley, E. G.; Albert, J. N. L.; Sullivan, M. O.; Epps, I. I. I. T. H. *Chem. Soc. Rev.* **2013**, *42*, 7057−7071.

(25) Doring, A.; Birnbaum, W.; Kuckling, D. *Chem. Soc. Rev.* **2013**, *42*, 7391−7420.

(26) Warren, N. J.; Derry, M. J.; Mykhaylyk, O. O.; Lovett, J. R.; Ratcliffe, L. P. D.; Ladmiral, V.; Blanazs, A.; Fielding, L. A.; Armes, S. P. *Macromolecules* **2018**, *51*, 8357–8371.

(27) Constantinou, A. P.; Sam-Soon, N. F.; Carroll, D. R.; Georgio, T. K. *Macromolecules* **2018,** *51*, 7019–7031.

(28) Cui, Q. L.; Wu, F. P.; Wang, E. J. *J. Phys. Chem. B* **2011,** *115*, 5913–5922.

(29) Umapathi, R.; Venkatesu, P. *J. Colloid Interf. Sci.* **2017,** *485*, 183–191

(30) Yildirim, T.; Traeger, A.; Sungur, P.; Hoeppener, S.; Kellner, C.; Yildirim, I.; Pretzel, D.; Schubert, S.; Schubert, U. S. *Biomacromolecules* **2017,** *18*, 3280–3290.

(31) Zhu, Y. C.; Batchelor, R.; Lowe, A. B.; Roth, P. J., *Macromolecules* **2016,** *49*, 672–680.

(32) Baddam, V.; Aseyev, V.; Hietala, S.; Karjalainen, E.; Tenhu, H. *Macromolecules* **2018**, *51*, 9681–9691.

(33) Penfold, N. J. W.; Whatley, J. R.; Armes, S. P., *Macromolecules* **2019** *52*, 1653–1662.

(34) Abboud, J.-Luis M.; Foces-Foces, C.; Notario, R.; Trifonov, Rostislav E.; Volovodenko, Anna P.; Ostrovskii, Vladimir A.; Alkorta, I.; Elguero, J. *Eur. J. Org. Chem.* **2001**, *2001*, 3013–3024.

(35) Kolb, H. C.; Sharpless, K. B. *Drug Discovery Today* **2003**, *8*, 1128–1137.

(36) Abarca B., Ballesteros-Garrido R. (2014) *1,2,3-Triazoles Fused to Aromatic Rings* in *Chemistry of 1,2,3-triazoles.* Dehaen W., Bakulev V., Eds., *Topics in Heterocyclic Chemistry,* 2014, vol 40, Springer, Cham.

(37) Schulze, B.; Schubert, U. S. *Chem. Soc. Rev.* **2014**, *43*, 2522-2571.

(38) McDonald, K. P.; Hua, Y.; Flood, A. H. Gale, P. A., Dehaen, W., Eds.; Springer Berlin Heidelberg: Berlin, Heidelberg, 2010, pp 341–366.

(39) Ghosh, K.; Panja, A.; Panja, S. *New J. Chem.* **2016**, *40*, 3476–3483.

(40) Jung, S.-H.; Ryu, J.; Sohn, D.; Lee, H.-i. *Polym. Chem.* **2012**, *3*, 1002–1006.

(41) Hua, Y.; Flood, A. H. *Chem. Soc. Rev.* **2010**, *39*, 1262–1271.

(42) Kanao, M.; Matsuda, Y.; Sato, T. *Macromolecules* **2003**, *36*, 2093–2102.

(43) Hashidzume, A.; Kawaguchi, A.; Tagawa, A.; Hyoda, K.; Sato, T. *Macromolecules* **2006**, *39*, 1135–1143.

(44) Kawata, T.; Hashidzume, A.; Sato, T. *Macromolecules* **2007**, *40*, 1174–1180.

(45) Sato, T.; Matsuda, Y. *Polym. J.* **2009**, *41*, 241–251.

(46) Mishra, V.; Jung, S.-H.; Park, J. M.; Jeong, H. M.; Lee, H.-i. *Macromol. Rapid Commun.* **2014**, *35*, 442–446.

(47) van Os, N. M.; Haak, J. R.; Rupert, L. A. M. Elsevier: Amsterdam, 1993.

(48) Nakano, S.; Hashidzume, A.; Sato, T. *Beilstein J. Org. Chem.* **2015**, *11*, 1037–1042.

(49) Obadia, M. M.; Drockenmuller, E. *Chem. Commun.* **2016**, *52*, 2433–2450.

Chapter 3

Emission Properties of Diblock Copolymers Composed of Poly(ethylene glycol) and Dense 1,2,3-Triazole Blocks

3-1. Introduction

As demonstrated that 1,2,3-triazole is an interesting nitrogen-rich heterocycle.[1–3] In 2002, the advent of copper(I)-catalyzed azide-alkyne cycloaddition (CuAAC) provides a straightforward strategy to produce 1,2,3-triazoles. The facile accessibility, coupled with the structural and physicochemical uniqueness, has made 1,2,3-triazole an attractive motif to develop functional materials. One of the particular interests is chemosensors,[4–9] by incorporating 1,2,3-triazole moieties to change the emission characteristics of appended fluorophore.[10-13] Azide-based fluorogenic probes are the typical examples, in which non-fluorescence azide-probes were activated by conversion to the corresponding triazoles.[14-16] However, most of these fluorescent materials share similar structures, which are azide or 1,2,3-triazole groups connected to an appended fluorophore.[17] The photophysical properties of 1,2,3-triazole and its derivatives have been an underexamined subject.

In Chapter 2, diblock copolymers, EG*m*-*b*-AP*n,* and EG*m*-*b*-AB*n*, have

been synthesized to investigate the properties of AP*n* block in solution. Unexpectedly, these diblock copolymer samples emitted fluorescence in solution state. EG*m*-*b*-AP*n* is fluorescent by itself although AP*n* block, in which 1,2,3-triazole moieties are connected through a methylene, is not conjugated. Fluorescent polymers have been widely applied to important fields, e.g., molecular sensors,[18-20] nonlinear optical materials,[20,21] and organic electroluminescence,[20,22] a new type of fluorescent polymers should be developed.

In this chapter, the photophysical properties of EG*m*-*b*-AP*n* are investigated by absorption and steady-state fluorescence spectroscopies. Interestingly, the emission of EG*m*-*b*-AP*n* can be easily tuned from ultraviolet to green fluorescence by changing the excitation wavelength. This enables fine-tuning of its optical property without changing the chromophore. We have also discussed the fluorescence behavior of EG*m*-*b*-AP*n* by comparing the experimental data with the results of density functional theory calculation. The experimental data have exhibited that AP*n* block is an intrinsic fluorophore. Moreover, the block copolymers show a fluorescence response to metal ions, e.g., Cu^{2+}.

3-2. Materials and Methods

Materials. 3-Bromo-1-propyne (BrP), sodium azide (NaN_3), copper(II) sulfate pentahydrate ($CuSO_4 \cdot 5H_2O$), and sodium (+)-ascorbate (NaAsc) were

purchased from FUJIFILM Wako Pure Chemical Co. (Osaka, Japan). Poly(ethylene glycol) (PEG) monomethyl ether (M_n ~750 and 2000, EG18 and EG45, respectively) and *N*,*N*-dimethylformamide (DMF) (≥99.9%) were purchased from Sigma-Aldrich (St. Louis, MO, USA). Solvents (e.g., acetone, toluene, dichloromethane, diethyl ether, and DMF), were purchased from FUJIFILM Wako Pure Chemical Co. (Osaka, Japan). Water was purified with a Millipore Milli-Q system. All the reagents were used without further purification.

Measurements. ^{1}H NMR spectra were recorded on a JEOL JNM ECA500 spectrometer using $CDCl_3$ or DMSO-d_6 as a solvent. Chemical shifts were referenced to the solvent value (7.26 and 2.50 ppm for $CDCl_3$ and DMSO-d_6, respectively). Size exclusion chromatography (SEC) measurements were carried out at 40 °C on a TOSOH HLC-8320GPC equipped with a TOSOH TSKgel SuperAWM-H column, using DMSO containing 10 mM LiBr as eluent at a flow rate of 0.4 mL min^{-1}. Molecular weights were calibrated with PEG and poly(ethylene oxide) (PEO) standards (Scientific Polymer Products, Inc., Ontario, NY, USA). All sample solutions for SEC were filtrated with a DISMIC-13JP PTFE 0.50 μm filter (ADVANTEC, Tokyo, Japan) just prior to injection. UV–visible absorption spectra were collected on a HITACHI U-410 0 spectrophotometer by using a 1.0 cm path length quartz cuvette at room temperature. Fluorescence measurements were performed on a HITACHI F-2500 equipped with a single

cuvette reader at room temperature. The slit widths for both the excitation and emission sides were kept at 5.0 nm during measurement. Absolute quantum yields (Φ) were evaluated with a Hamamatsu Photonics C9920-02 absolute photoluminescence (PL) quantum yield measurement system. Pulse field gradient spin-echo (PGSE) NMR data were obtained on a Bruker AVANCE 700 NMR spectrometer at 30 °C using *N*,*N*-dimethylformamide-d_7 (DMF-d_7) as a solvent. The bipolar pulse pair stimulated echo (BPPSTE) sequence was applied.[31–33] The strength of pulsed gradients (g) was increased from 0.96 to 47.2 gauss cm^{-1}. The time separation of pulsed field gradients (Δ) and their duration (δ) were 0.05 and 0.004 s, respectively. The sample was not spun, and the airflow was disconnected. The shape of the gradient pulse was rectangular, and its strength was varied automatically during the course of the experiments.

Preparation of Monopropargyl-Terminated Poly(ethylene glycol) (EGm-P). A typical procedure for EG*m*-P is described below.

EG45 (15.02 g, 7.5 mmol) was added in toluene (50 mL) with stirring at room temperature for 0.5 h to make sure that all the EG45 was dissolved in toluene. Then NaOH (1.83 g, 45.8 mmol) and BrP (1.2 mL, 15.0 mmol) were added. After stirring for 4 h, BrP (1.2 mL, 15.0 mmol) and NaOH (1.80 g, 45.0 mmol) were further added to the reaction mixture with continuous stirring for 26 h. The colorless precipitate was removed from the reaction mixture by filtration, and the

solvent was then removed under reduced pressure. The residue was dissolved in an aqueous solution of NaCl (5.1 wt %, 100 mL). Then the product was extracted from the aqueous solution with CH_2Cl_2 (3 × 50 mL). The organic layers were combined. The combined organic phase was washed with an aqueous solution of NaCl (5.1 wt %, 2 × 100 mL). After drying the organic phase with anhydrous $MgSO_4$, the $MgSO_4$ was removed by filtration. The solvent was removed under reduced pressure to obtain crude product. Finally, the product was purified by reprecipitation with CH_2Cl_2 and hexane twice. The final product was recovered as pale yellow gel after drying under vacuum at 45 °C for 24 h; yield 13.1 g (86.4%).

Preparation of EGm-b-APn Block Copolymers. A typical example of the preparation of diblock copolymers of PEG and dense 1,2,3-triazole blocks (EG*m*-*b*-AP*n*, where *m* and *n* denote the degrees of polymerization) is described below.

A solution of EG45-P (2.52 g, 1.25 mmol) in DMF (5 mL), $CuSO_4 \cdot 5H_2O$ (0.030 g, 0.125 mmol), and NaAsc (0.050 g, 0.25 mmol) were added to a 100 mL flask under a nitrogen atmosphere. The mixture was stirred for 5 min. Then, NaN_3 (1.95 g, 30 mmol) and BrP (2.8 mL, 25 mmol, 80 wt % in toluene) were added to the reaction mixture. The reaction mixture was warmed with an oil bath at 80 °C with stirring. After 72 h, the reaction mixture was added to DMF (50 mL). The precipitate was removed by filtration. The solution was then passed through a neutral Al_2O_3 column. The volatile fraction was removed under reduced pressure.

The polymer obtained, EG45-*b*-AP22, was purified by reprecipitation by using pairs of solvents (i.e., a DMF/CH_2Cl_2 (1/20, *v*/*v*) mixed solvent and acetone three times). The final product was dried at 80 °C under vacuum; brown solid, 1.2 g, 34.9%.

Density Functional Theory (DFT) Calculations. To investigate the highest-occupied and lowest-unoccupied molecular orbitals (HOMO and LUMO, respectively), DFT calculations were carried out for model systems of EG*m*-*b*-AP*n* using the Gaussian 09 program.[29] In all the calculations, DFT with B3LYP functional was used, and 6-31+G(d) basis sets were applied for the hydrogen, carbon, nitrogen, and oxygen atoms. All the geometries of the model systems were fully optimized.

3-3. Results and Discussion

Samples of EG*m*-*b*-AP*n* were prepared by CuAAC polymerization of 3-azido-1-propyne (AP) in the presence of PEG modified with a propargyl group at one end (EG*m*-P), which is the same as the method in Chapter 2. Table 3-1 summarizes the basic characteristics of EG*m*-*b*-AP*n* samples. These samples were characterized by SEC and ^{1}H NMR. Our previous work has demonstrated that AP homopolymer is insoluble in all the common solvents examined, e.g. DMF, DMSO, NMP, methanol, acetone, THF, chloroform, and toluene.[24,25] Thus, the

solubility of the EG*m*-*b*-AP*n* diblock copolymer samples was examined, and the results are summarized in Table 3-2. Because of the EG*m* block, the EG*m*-*b*-AP*n* samples were soluble in many common solvents. Especially, the samples were well soluble in polar organic solvents.

Table 3-1. Molecular characteristics of EG*m*-*b*-AP*n* prepared by CuAAC polymerization.

polymer code [a]	$M_n \times 10^{-3}$ [b]	$M_n \times 10^{-3}$ [c]	M_w/M_n [c]
EG18-*b*-AP4	1.1	1.5	1.26
EG18-*b*-AP12	1.8	3.3	1.98
EG45-*b*-AP6	2.5	2.7	1.40
EG45-*b*-AP22	3.6	2.5	2.37

a. The numbers denote DP determined by ^{1}H NMR spectroscopy. *b*. Determined by ^{1}H NMR. *c*. Determined by SEC in DMSO at 40 °C calibrated with PEG and PEO standards.

Table 3-2. Results of solubility test for EG*m*-*b*-AP*n* samples.[a]

solvent	EG18-*b*-AP4	EG18-*b*-AP12	EG45-*b*-AP6	EG45-*b*-AP22
water	++	+	++	+
methanol	+	–	++	+
acetic acid	++	++	++	++
NMP	++	++	++	++
DMSO	++	++	++	++
DMF	++	++	++	++
acetonitrile	++	+	++	+
acetone	++	–	+	–
dicholromethane	++	++	++	+
chloroform	++	++	++	+
pyridine	++	++	++	+
THF	+	–	+	–
ethyl acetate	+	–	–	–
toluene	–	–	–	–

a. "++", "+", and "–" denote well soluble (≥ 1 wt%), slightly soluble (< 1 wt%), and insoluble, respectively.

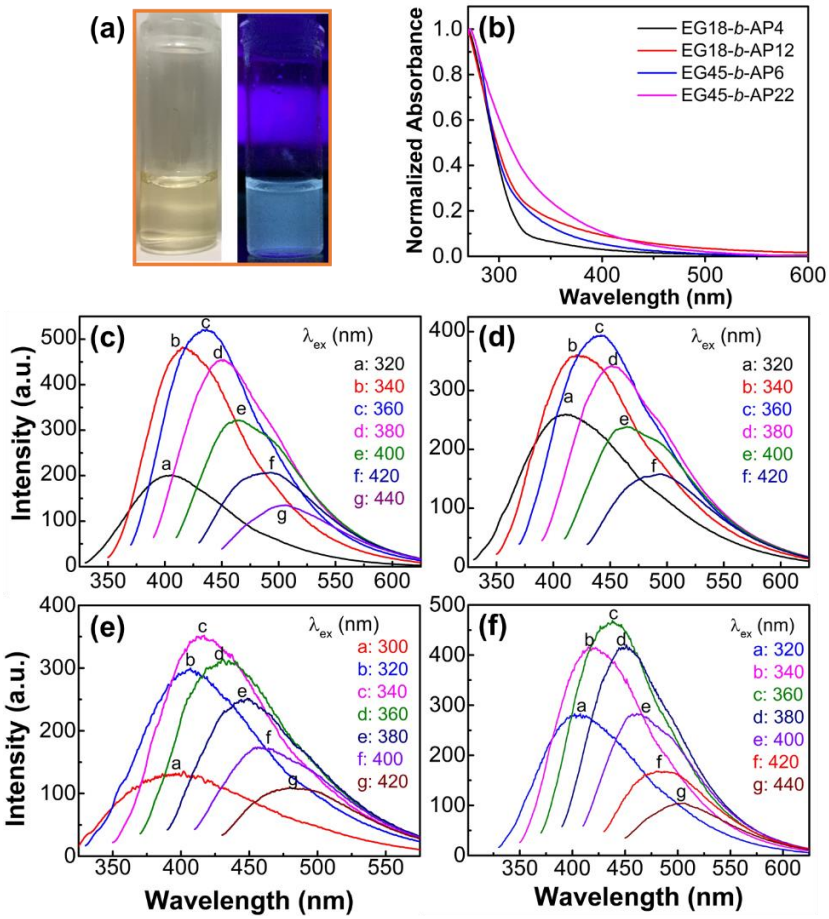

Figure 3-1. Photographs of EG45-*b*-AP22 in DMF at 1.0 g L^{-1} under visible (left) and UV (λ = 365 nm) light (right) (a), UV-visible absorption spectra normalized at 270 nm for 1.00 g L^{-1} solutions of EG*m*-*b*-AP*n* in DMF (b), and steady-state fluorescence spectra for 1.00 g L^{-1} solutions of EG18-*b*-AP4 (c), EG18-*b*-AP12 (d), EG45-*b*-AP6 (e), and EG45-*b*-AP22 (f) in DMF with excitation at varying wavelengths.

When a solution of EG*m*-*b*-AP*n* in DMF was measured by dynamic light scattering in order to characterize the polymer chains in the molecularly dispersed state, emission from the solution was observed. Thus, the photophysical behavior of solutions of the EG*m*-*b*-AP*n* samples in DMF was examined by absorption and steady-state fluorescence spectroscopy. As can be seen in Figure 3-1a, a solution of EG45-*b*-AP22 in DMF emits blue fluorescence under irradiation with 360 nm UV light. Figure 3-1b displays UV-visible absorption spectra for solutions of the EG*m*-*b*-AP*n* samples in DMF. These spectra exhibit absorption in the wavelength range of 270 – 450 nm, which is ascribable to the dense 1,2,3-triazole block. It should be noted here that EG45-*b*-AP22 shows absorption bands in the near UV and visible regime of 300 – 500 nm, which are stronger compared to that for EG45-*b*-AP6. This observation indicates that a longer dense 1,2,3-triazole block absorbs light of a longer wavelength. Figures 3-1c to 3-1f indicate steady-state fluorescence spectra for DMF solutions of EG*m*-*b*-AP*n* with excitation at varying wavelengths from 300 to 440 nm. These spectra exhibit that the solutions emit fluorescence of a wavelength increasing from UV to green with increasing excitation wavelength. This may be because the EG*m*-*b*-AP*n* samples possess a rather broad molecular weight distribution, and AP*n* blocks of different lengths are excited at different wavelengths.[26,27] The excitation and emission bands of AP*n* block are dependent on the degree of

polymerization. Since EG*m*-P did not emit fluorescence,[28,29] it is likely that the emission observed is from the dense 1,2,3-triazole block. The absolute fluorescence quantum yields were evaluated for the EG*m*-*b*-AP*n* samples in DMF, acetonitrile, and water. As listed in Table 3-3, the quantum yield ranges 1.4 – 3.4 %, indicating that the quantum yields in DMF are higher than those in the other solvents.

Table 3-3. Fluorescence quantum yields for the EG*m*-*b*-AP*n* samples in DMF, acetonitrile, and water (1.00 g L^{-1}).

	Φ		
polymer code	in DMF	in acetonitrile	in water
EG18-*b*-AP4	0.034	0.020	0.018
EG18-*b*-AP12	0.020	—	—
EG45-*b*-AP6	0.029	0.019	0.014
EG45-*b*-AP22	0.024	—	—

Recently, aggregation-induced emission (AIE) has attracted increasing interest from researchers because of its potential application for molecular sensors.[30] Some examples of AIE from polymers possessing no aromatic moieties have been reported. It is important to know whether or not the emission

observed from EG*m*-*b*-AP*n* is AIE. The association behavior of EG*m*-*b*-AP*n* was preliminarily investigated in DMF by PGSE NMR.[31] The PGSE NMR data are presented in Figure 3-2a. The intensity data practically obey a straight line at four different concentrations, indicative of a unimodal distribution. The unimodal distribution is confirmed by DOSY data as can be seen in Figure 3-3.

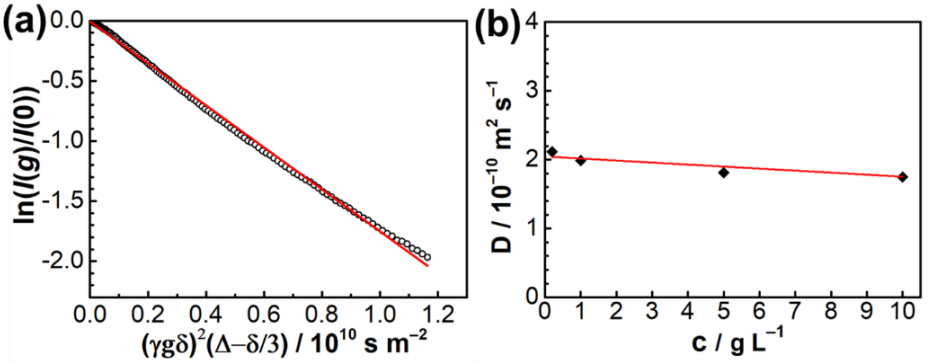

Figure 3-2. PGSE NMR data for 10.0 g L–1 solution of EG45-b-AP22 in DMF-d_7 (a) and the concentration dependencies of D.

From the slopes of straight lines, apparent diffusion coefficients (D) were evaluated and plotted in Figure 3-2b against the polymer concentration. The diffusion coefficient (D_0) was determined by extrapolation to zero concentration. Using Einstein–Stokes equation, the hydrodynamic radius (R_H) was calculated to be 1.35 nm for EG45-*b*-AP22. The R_H value is almost the same as that for PEG of the same molecular weight, indicating that most of EG45-*b*-AP22 chains are

molecularly dispersed in DMF. As discussed in a later subsection, the fluorescence intensity decreased markedly when a small amount of water was added to a solution of EG*m*-*b*-AP*n* in DMF to induce aggregation because water is a rather poor solvent for EG*m*-*b*-AP*n*. This observation confirms that the emission observed for DMF solutions is from EG*m*-*b*-AP*n* in the molecularly dispersed state.

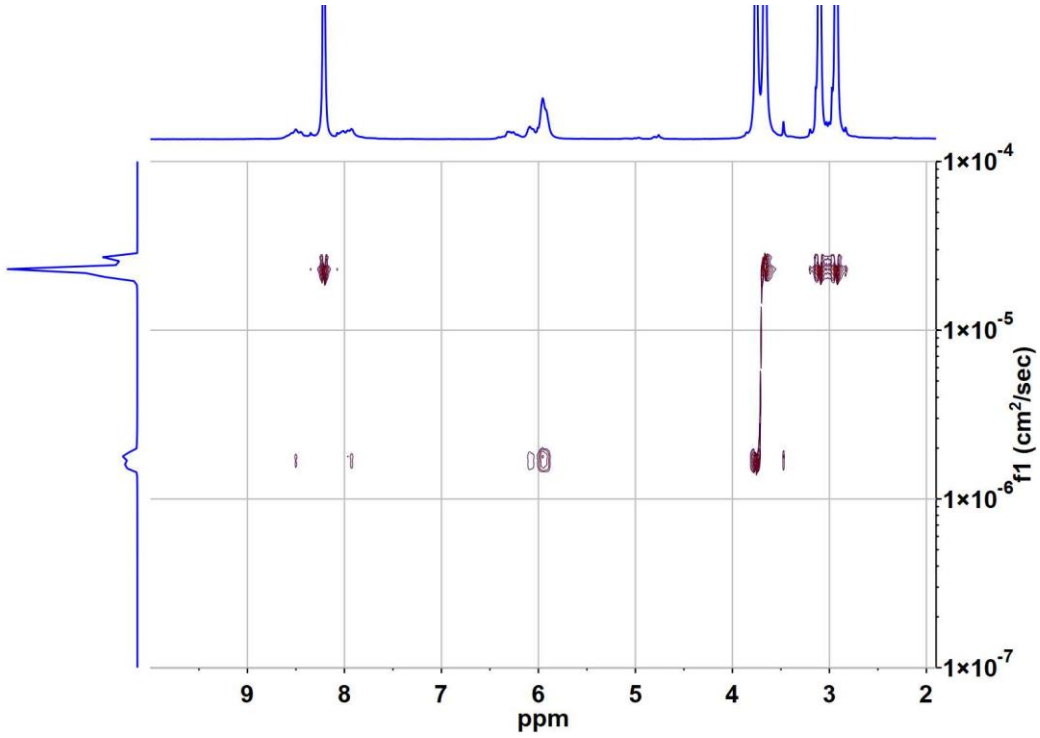

Figure 3-3. DOSY spectrum for a 10.0 g L^{-1} solution of EG45-*b*-AP22 in DMF-d_7 at 298 K.

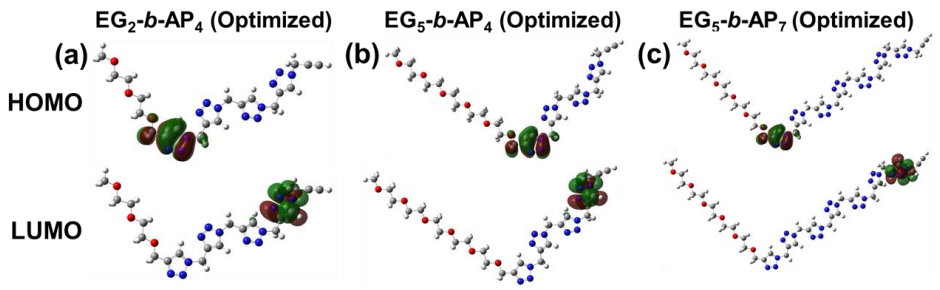

Figure 3-4. Optimized structures as well as the HOMO and LUMO for EG2-*b*-AP4 (a), EG5-*b*-AP4 (b), and EG5-*b*-AP7 (c) obtained by DFT calculations using a B3LYP/6-31+G(d) basis set with a Gaussian'09 program (Blue: N; red: O; grey: C; white: H).

To understand the detail mechanism of the fluorescence observed, the HOMO and LUMO of EG*m*-*b*-AP*n* were estimated by DFT calculations. As shown in Figure 3-4, the HOMO is located on the 1,2,3-triazole unit directly connecting the PEG block. On the other hand, the LUMO is located on the terminal 1,2,3-triazole unit. These observations indicate that the emission is from the dense 1,2,3-triazole block. The absorption and fluorescence wavelengths were also evaluated by DFT calculation, as listed in Table 3-4. The length of PEG block has no or only a little effect on the absorption and fluorescence wavelengths. On the other hand, as the degree of polymerization of AP*n* block is increased from 4 to 7, the absorption and fluorescence wavelengths become longer, i.e., a red shift.

The red shift is larger for fluorescence than that for absorption. These data indicate that the absorption and fluorescence wavelengths depend on the length of AP*n* block. It is noteworthy that the fluorescence wavelength calculated agrees well with the fluorescence maximum observed.[32,33] On the basis of these observations, it is concluded that the emission from solutions of EG*m*-*b*-AP*n* is not AIE, and the fluorescence from the dense 1,2,3-triazole blocks in the molecularly-dispersed state.

Table 3-4. Time-dependent DFT -predicted properties of models of EG*m*-*b*-AP*n*.

Model	Abs. [a] / nm	Emission [b] / nm
EG2-*b*-AP4	231.1	456.6
EG5-*b*-AP4	231.4	455.7
EG5-*b*-AP7	237.1	473.9

a. Energy (TDDFT) using the optimized structure in ground state. *b*. Optimization (TDDFT, root = 1) using the optimized structure in ground state.

The effects of the solvent and polymer concentration on fluorescence behavior were examined. Figure 3-5a displays fluorescence spectra for EG45-*b*-AP22 in different solvents with excitation at 360 nm. The block copolymer

shows an emission band depending on the solvent used. When a small amount of water was added to the solution of EG45-*b*-AP22 in DMF, the fluorescence intensity decreased remarkably. As can be seen in Table 2, water is not a good solvent for EG45-*b*-AP22 compared to DMF and DMSO. Since our light scattering data indicated that EG45-*b*-AP22 forms aggregates in water (Chapter 2), it is likely that the aggregation of EG45-*b*-AP22 quenches fluorescence. Figure 3-5b exhibits fluorescence spectra for EG45-b-AP22 in a mixed solvent of DMF and THF, a poor solvent, indicating that the fluorescence intensity decreases with increasing the THF content. As can be seen in Figure 3-5c, the fluorescence intensity decreases with increasing the polymer concentration from 1 to 20 g L^{-1}. These observations confirm that aggregation quenches fluorescence.

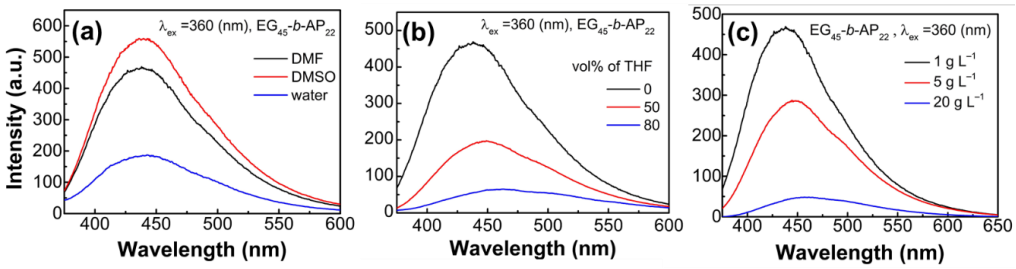

Figure 3-5. Steady-state fluorescence spectra for solutions of EG45-*b*-AP22 (1.00 g L^{-1}) in water, DMF, and DMSO (a), in mixed solvent of DMF and THF with different THF contents (b), and in DMF at different concentrations with excitation at 360 nm (c).

As described in Chapter 1, it is known that 1,2,3-triazole moieties can act as metal ligands.[34] It is thus expected that the fluorescence behavior of EG*m*-*b*-AP*n* diblock copolymers should be responsive to the metal ion added. In this study, the effect of addition of Na^+, Zn^{2+}, or Cu^{2+} was investigated. Figure 3-6 shows fluorescence spectra for an aqueous solution of EG18-*b*-AP10 in the absence and presence of Na^+, Zn^{2+}, or Cu^{2+}. In the presence of Na^+ or Zn^{2+}, the fluorescence spectra are almost the same as that in the absence. In the presence of Cu^{2+}, however, the fluorescence intensity is markedly weaker. This may be because dense 1,2,3-triazole moieties coordinate Cu^{2+} ions and fluorescence are quenched through the heavy metal effect. These observations indicate that the fluorescence of EG*m*-*b*-AP*n* can be applicable to a molecular sensor of metal ions.

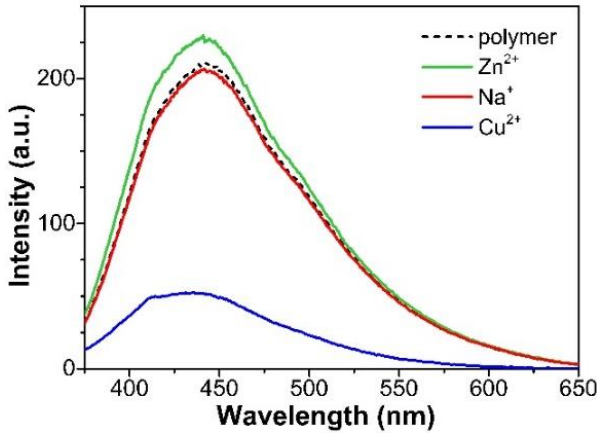

Figure 3-6. Steady-state fluorescence spectra for a 1.0 g L^{-1} aqueous solution of EG18-*b*-AP10 with excitation at 360 nm in the absence and the presence of 0.10 M Na^+, 0.10 M Zn^{2+}, or 0.005 M Cu^{2+}.

3-4. Conclusions

The solubility and phogophysical properies of dense triazole-based block copolymers, EG*m*-*b*-AP*n*, in solution state were studied. The incorporation of EGm block significantly enhanced the solubility of bock copolymers in common polar solvents. Their solubility decreased with increasing the length of AP*n* block. Significantly, without attachment of any extra fluorophore, the as-prepared block copolymers emitted fluorescence in solution state. The emission of block copolymers was tunable from ultraviolet to green fluorescence by changing the excitation wavelength presumably because a longer AP*n* block was excited at a longer wavelength. PGSE NMR analysis and theoretical calculation indicated that the copolymers were molecularly dispersed in DMF-d_7 and AP*n* block was an intrinsic fluorophore. It is noteworthy that the emission of block copolymer was responsive to metal ions because of the interaction with dense 1,2,3-triazole blocks dependent on the ionic species.

References

(1) Lehn, J. M. *Science* **1993**, *260*, 1762–1764.

(2) Abboud, J. L. M.; Foces-Foces, C.; Notario, R.; Trifonov, R. E.; Volovodenko,

A. P.; Ostrovskii, V. A.; Alkorta, I.; Elguero, J. *Eur. J. Org. Chem.* **2001**, 3013–3024.

(3) Schulze, B.; Schubert, U. S. *Chem. Soc. Rev.* **2014**, *43*, 2522–2571.

(4) Reynhout, I. C.; Löwik, D. W.; van Hest, J. C.; Cornelissen, J. J.; Nolte, R. J. *Chem. Commun.* **2005**, 602–604.

(5) Qing, G.; Xiong, H.; Seela, F.; Sun, T. *J. Am. Chem. Soc.* **2010**, *132*, 15228–15232.

(6) Wu, J.; Liu W.; Han H.; Sun R.; Xie M.; Liao X. *Polym. Chem.* **2015**, *6*, 4801–4808.

(7) Jourdain, A.; Serghei, A.; Drockenmuller, E. *ACS Macro Lett.* **2016**, *5*, 1283–1286.

(8) König, N. F.; Al Ouahabi, A.; Poyer, S., Charles, L.; Lutz, J. F. *Angew. Chem. Int. Ed.* **2017**, *56*, 7297–7301.

(9) Pulst, M.; Samiullah, M. H.; Baumeister, U.; Prehm, M.; Balko, J.; Thurn-Albrecht, T.; Busse, K.; Golitsyn, Y.; Reichert, D.; Kressler, J. *Macromolecules* **2016**, *49*, 6609–6620.

(10) Hao, E.; Meng, T.; Zhang, M.; Pang, W.; Zhou, Y.; Jiao, L. *J. Phys. Chem. A* **2011**, *115*, 8234–8241.

(11) Lau, Y. H.; Rutledge, P. J.; Watkinson, M.; Todd, M. H. *Chem. Soc. Rev.* **2011**, *40*, 2848–2866.

(12) Nadler, A.; Schultz, C. *Angew. Chem. Int. Ed.* **2013**, *52*, 2408–2410.

(13) Shie, J. J.; Liu, Y. C.; Hsiao, J. C.; Fang, J. M.; Wong, C. H. *Chem. Commun.* **2017**, *53*, 1490–1493.

(14) Shie, J. J.; Liu, Y. C.; Lee, Y. M.; Lim, C.; Fang, J. M.; Wong, C. H. *J. Am. Chem. Soc.* **2014**, *136*, 9953–9961.

(15) Shieh, P.; Dien, V. T.; Beahm, B. J.; Castellano, J. M. *J. Am. Chem. Soc.* **2015**, *137*, 7145–7151.

(16) Xie, F.; Sivakumar, K.; Zeng, Q. B.; Bruckman, M. A.; Hodges, B.; Wang, Q. *Tetrahedron* **2008**, *64*, 2906–2914.

(17) Le Droumaguet, C.; Wang, C.; Wang, Q. *Chem. Soc. Rev.* **2010**, *39*, 1233–1239.

(18) Toal, S. J.; Trogler, W. C. *J. Mater. Chem.* **2006**, *16*, 2871–2883.

(19) Thomas, S. W.; Joly, G. D.; Swager, T. M. *Chem. Rev.* **2007**, *107*, 1339–1386.

(20) Liu, J.; Lam, J. W. Y.; Tang, B. Z. *Chem. Rev.* **2009**, *109*, 5799–5867.

(21) Willets, K. A.; Nishimura, S. Y.; Schuck, P. J.; Twieg, R. J.; Moerner, W. E.

Acc. Chem. Res. **2005**, *38*, 549–556.

(22) Yang, X.; Xu, X.; Zhou, G. *J. Mater. Chem. C* **2015**, *3*, 913–944.

(23) Zhu, S.; Song, Y.; Shao, J.; Zhao, X.; Yang, B. *Angew. Chem. Int. Ed.* **2015**, *54*, 14626–14637.

(24) Hashidzume, A.; Nakamura, T.; Sato, T. *Polymer* **2013**, *54*, 3448–3451.

(25) Nakano, S.; Hashidzume, A.; Sato, T. *J. Org. Chem.* **2015**, *11*, 1037–1042.

(26) Qiao, Z.-A.; Huo, Q.; Chi, M.; Veith, G. M.; Binder, A. J.; Dai, S *Adv. Mater.* **2012**, *24*, 6017–6021.

(27) Zhu, S.; Wang, L.; Zhou, N.; Zhao, X.; Song, Y.; Maharjan, S.; Zhang, J.; Lu, L.; Wang, H.; Yang, B. *Chem. Commun.* **2014**, *50*, 13845–13848.

(28) Zhang, X.; Wang, S.; Xu, L.; Feng, L.; Ji, Y.; Tao, L.; Li, S.; Wei, Y. *Nanoscale* **2012**, *4*, 5581–5584.

(29) Frisch, M. J.; Trucks, G. W.; Schlegel, H. B.; Scuseria, G. E.; Robb, M. A.; Cheeseman, J. R.; Scalmani, G.; Barone, V.; Mennucci, B.; Petersson, G. A.*, et al. Gaussian 09, Revision, B.01*, Scientific Research: Wallingford CT, 2009.

(30) Mei, J.; Leung, N. L. C.; Kwok, R. T. K.; Lam, J. W. Y.; Tang, B. Z. *Chem. Rev.* **2015**, *115*, 11718–11940.

(31) Price, W. S.; Ide, H.; Arata, Y. *J. Phys. Chem. A* **1999**, *103*, 448–450.

(32) Sarkar, S.; Mondal, A.; Tiwari, A.K.; Shunmugam, R. *Chem. Commun.* **2012**, *48*, 4223–4225.

(33) Yan, J.; Wang, R.; Pan, D.; Yang, R.; Xu, Y.; Wang, L.; Yang, M. *Polym. Chem.* **2016**, *7*, 6241–6249.

(34) Xu, Q.; Lee, K. M.; Wang, F.; Yoon, J. *J. Mater. Chem.* **2011**, *21*, 15214–15217.

Chapter 4

Tough and Strong Self-Healing Elastomer Formed from Triblock Copolymers Possessing Dense 1,2,3-Triazole Blocks

4-1. Introduction

Exploiting dynamic noncovalent interaction to develop new polymeric materials that are strong, stretchable, and healable has attracted a dramatic growth of interest in recent years.[1–3] The reversible features of noncovalent interactions allow ones to construct structurally dynamic polymeric systems that can adapt their structure and therefore show reversible healing ability.[4,5] Recently, several polymers with high mechanical properties have been developed by utilizing hydrogen bonding,[6–8] metal–ligand interaction,[9–11] host–guest interaction,[12–14] and π–π stacking.[15,16] As mentioned in Chapter 1, 1,2,3-triazole can offer diverse supramolecular interactions, including hydrogen bonding, π–π stacking, anion complexation, metal ion coordination, and dipole–dipole interaction.[17] In Chapter 2, diblock copolymer, EG*m*-*b*-AP*n*, forms aggregates through the strong dipole–dipole interaction of the dense triazole blocks, in which individual triazole rings interact cooperatively. This chapter deals with the concept that takes advantage of the strong dipole–dipole interactions to achieve high strength,

stretchability, and healing ability.

In this chapter, BAB type-triblock copolymers, in which B block is associative one, are prepared from PEG and dense triazole blocks (poly(3-azido-1-propyne)-*block*-poly(ethylene glycol)-*block*-poly(3-azido-1-propyne) (AP*n*-*b*-EG*m*-*b*-AP*n*, Scheme 4-1)), aiming at supramolecular materials that offers good strength, stretchability, and healing ability based on the strong dipole–dipole interaction of the dense triazole blocks.

Scheme 4-1. Synthetic Route of AP*n*-*b*-EG*m*-*b*-AP*n* Triblock Copolymers

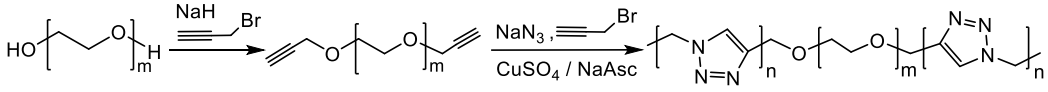

4-2. Materials and Methods

Materials. Sodium azide (NaN_3), sodium (+)-ascorbate (NaAsc), and copper(II) sulfate pentahydrate ($CuSO_4$•$5H_2O$), (≥ 99.9%) were purchased from FUJIFILM Wako Pure Chemical Co. (Osaka, Japan). 3-Bromo-1-propyne (BrP, 80wt% in toluene) and poly(ethylene glycol) (PEG) (M_n = 1500 and 3000, EG*m*, where *m* is the degree of polymerization (DP) of PEG) was purchased from Sigma-Aldrich (St. Louis, MO). Dithranol was purchased from ICN Biomedicals, Inc. (Aurora, OH). Solvents, i.e., acetone, toluene, dichloromethane, diethyl ether,

and *N*,*N*-dimethylformamide (DMF), were purchased from FUJIFILM Wako Pure Chemical Co. Water was purified by a Millipore Milli-Q system. All the reagents were used without further purification.

Measurements. ^{1}H NMR spectra were recorded on a JEOL JNM ECA500 spectrometer using $CDCl_3$ or dimethyl sulfoxide-d_6 (DMSO-d_6) as a solvent. Tetramethylsilane or the residual solvent signal was used as an internal standard. Size exclusion chromatography (SEC) measurements were carried out at 40 °C on a TOSOH HLC-8320GPC equipped with a TOSOH TSKgel SuperAWM-H column, using dimethyl sulfoxide (DMSO) containing 10 mM LiBr as eluent at a flow rate of 0.4 mL min^{-1}. Molecular weights were calibrated with PEG and poly(ethylene oxide) (PEO) standards (Scientific Polymer Products, Inc. (Ontario, NY)). All the SEC samples were passed through a 0.50 μm DISMIC JP050AN membrane filter (ADVANTEC (Tokyo, Japan)) just prior to measurements. MALDI-ToF mass spectrometry was conducted using a Shimadzu/KRATOS AXIMA-CFR spectrometer with dithranol as a matrix. A solution of matrix, dithranol (10.0 g L^{-1}, 2 μL), in acetone and a solution of sample (5.0 g L^{-1}, 2 μL) in acetone were applied to the target plate. ToF detection was performed using an appropriate accelerating voltage. Tensile testing was carried out by an Autograph AG-X plus (Shimadzu Co.) equipped with a 50 N load cell, at a strain rate of 10 mm s^{-1}. Small-angle X-ray scattering measurements (SAXS) measurements were

performed in transmission configuration on a SAXSLAB Ganesha instrument using Cu Kα (1.54 Å) radiation. The rheological measurements were conducted using an ARES G2 (TA Instruments, Tokyo, Japan) equipped with parallel plates of 4 mm in diameter. The temperature of the bottom plate was monitored by a thermocouple and regarded as the sample temperatures. Differential scanning calorimetry (TA 2500) was used to characterize the film thermal properties and was performed from –80 °C to 120 °C at a 10 °C min^{-1} heating rate under nitrogen flow.

Preparation of Dipropargyl-Terminated EGm (EGm-diP). A typical procedure for preparation of EG*m-di*P is described below.

EG68 (15.0 g, 5.0 mmol) was added in toluene (50 mL) with stirring at room temperature for 0.5 h to make sure that all PEG was dissolved in toluene. Then BrP (1.5 mL, 15.0 mmol) was added. Under stirring, NaH (0.72 g, 30.0 mmol) was added slowly. After stirring for 12 h, BrP (1.5 mL, 15.0 mmol) and NaH (0.72 g, 30.0 mmol) were further added to the reaction mixture with continuous stirring for 36 h. The inorganic precipitate was filtered out from the reaction mixture and the solvent was removed under reduced pressure. The residue was dissolved in an aqueous solution of NaCl (5.1 wt%, 100 mL). Then the product was extracted from the aqueous solution with CH_2Cl_2 (3 × 50 mL). The organic phases were combined. The combined organic layer was washed with an aqueous solution of NaCl (5.1%,

2 × 100 mL). After drying the organic phase with $MgSO_4$, the $MgSO_4$ was removed by filtration. The solvent was evaporated under reduced pressure and the product was dried under vacuum at 45 °C for 24 h. Pale yellow solid was obtained (13.8 g, 92% yield). Dichloromethane must be removed completely from EG18-P because it may react with NaN_3 to form diazidomethane in the next reaction. ^{1}H NMR (500 MHz, $CDCl_3$) δ (ppm): 4.23–4.17 (brs, 2H), 3.75–3.50 (br, 4H), 2.45–2.40 (brs, H).

Preparation of Triblock Copolymers APn-b-EGm-b-APn. A typical procedure of preparation of AP*n*-*b*-EG*m*-*b*-AP*n*, where *n* is DP of AP block, is described below.

A solution of EG68-*di*P (2.1 g, 0.7 mmol) in DMF (6 mL), $CuSO_4$•$5H_2O$ (0.0175 g, 0.07 mmol), and NaAsc (0.0198 g, 0.2 mmol) were added to a 100 mL flask under a nitrogen atmosphere. The mixture was stirred for 5 min. Then, NaN_3 (0.9751 g, 15 mmol) and BrP (0.84 mL, 7 mmol) were added to the reaction mixture. The reaction mixture was warmed with an oil bath thermostated at 80 °C with stirring. After 72 h, the reaction mixture was added to DMF (50 mL). The precipitate was removed by filtration. The volatile fraction was evaporated under reduced pressure. Then, dichloromethane (100 mL) was added and the precipitate was removed by centrifugation. The polymer obtained was dried at 60 °C under vacuum. Brown solid was obtained (1.6 g yield). ^{1}H NMR (500 MHz, DMSO-

d_6) δ (ppm): 8.49–7.54 (br, H), 6.16–5.45 (br, 2H), 4.75–4.35 (br, 2H), 3.75–3.31 (br, 4H).

4-3. Results and Discussion

Material Design and Characterization. The synthetic route to AP*n*-*b*-EG*m*-*b*-AP*n* is shown in Scheme 4-1. Two EG*m* samples, i.e. EG34 and EG68, were initially modified with two propargyl moieties at both the ends by reaction with BrP in the presence of NaH to obtain EG*m*-*di*P. The EG*m*-*di*P samples were characterized by ^{1}H NMR and MALDI-ToF mass spectra (Figures 4-1 and 4-2, respectively). MALDI-ToF mass spectra show only a series of signals EG*m*-*di*P, indicative of quantitative modification of the EG*m* with propargyl moieties. PDIs were measured by SEC to be 1.71 and 1.11 of EG34-*di*P and EG68-*di*P, respectively. Then, CuAAC polymerization of AP in the presence of EG*m*-*di*P was carried out in the same manner as that for the EG*m*-*b*-AP*n* diblock copolymers. A series of AP*n*-*b*-EG*m*-*b*-AP*n* samples were prepared at varying the molar ratios of BrP and EG*m*-*di*P. On the basis of characterization of AP*n*-*b*-EG*m*-*b*-AP*n* samples by ^{1}H NMR (Figure 4-3), attenuated total reflection FTIR (not shown), and SEC measurements, the basic characteristics of the copolymer samples were determined (Table 4-1). Noteworthily, the M_n values determined by SEC ($M_{n,SEC}$) are significantly higher than those determined by ^{1}H NMR ($M_{n,NMR}$). This may

be because AP*n*-*b*-EG*m*-*b*-AP*n* form intermolecular aggregates in DMSO, i.e., the eluent of SEC.

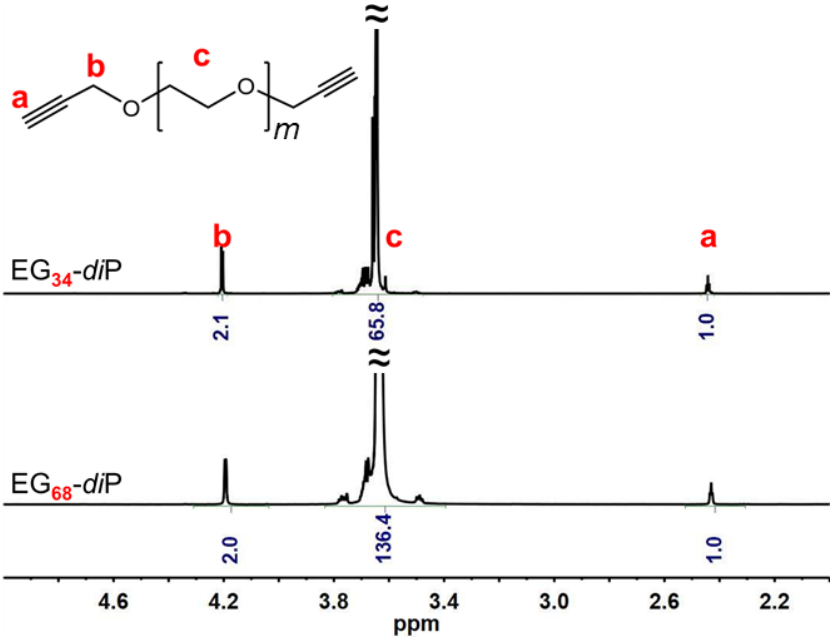

Figure 4-1. ^{1}H NMR spectra of EG*m*-*di*P in $CDCl_3$ (500 MHz, 25 °C).

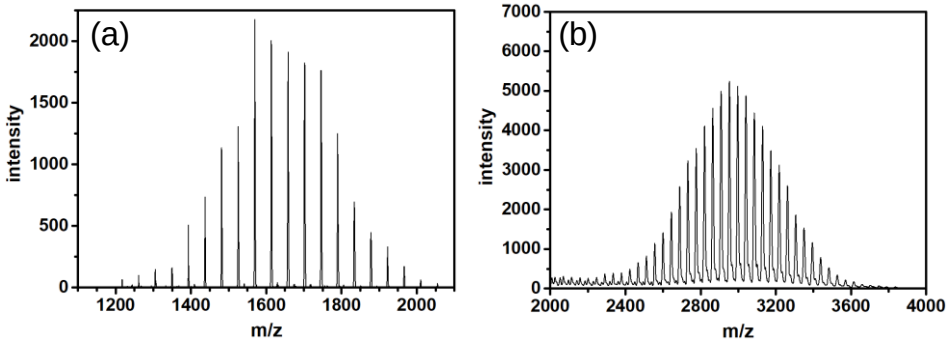

Figure 4-2. MALDI-ToF-MS for EG34-*di*P(a) and EG68-*di*P (b).

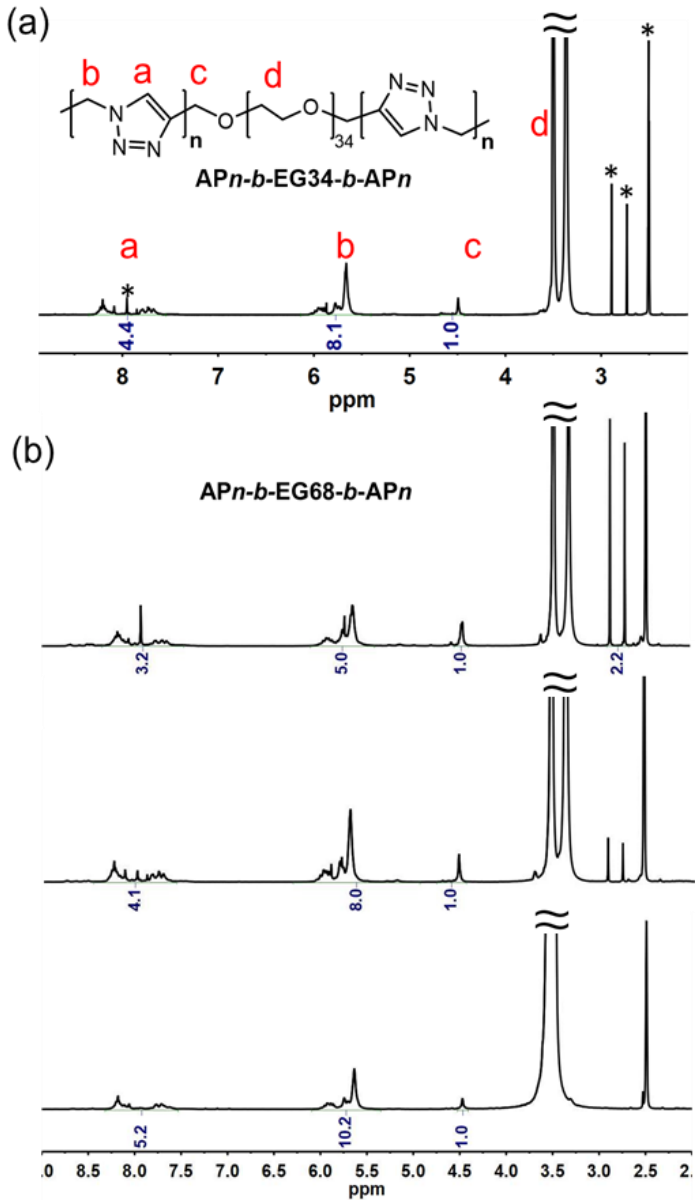

Figure 4-3. ^{1}H NMR spectra for AP*n*-*b*-EG34-*b*-AP*n* (a) and AP*n*-*b*-EG68-*b*-AP*n* in DMSO-d_6 (b). Using the ratio of area intensities of signals b and c, the *n* values were evaluated. Asterisks denote signals due to the residual solvents.

Table 4-1. Basic Characteristics of AP*n*-*b*-EG*m*-*b*-AP*n* Prepared in This Study

polymer code [a]	EG*m*-*di*P : BrP	$M_{n,NMR}$ [b] /10^3	$M_{n,SEC}$ [c] /10^3	M_w/M_n [c]
AP8-*b*-EG34-*b*-AP8	1 : 20	2.8	4.5	4.3
AP5-*b*-EG68-*b*-AP5	1 : 10	3.8	-	-
AP8-*b*-EG68-*b*-AP8	1 : 20	4.3	15.4	2.3
AP10-*b*-EG68-*b*-AP10	1 : 20	4.6	29.1	3.4

a. DP values were determined by ^{1}H NMR spectroscopy. *b*. Calculated from the DP data determined by ^{1}H NMR spectroscopy. *c*. Determined by SEC using DMSO as eluent. Molecular weights were calibrated with PEG and PEO standard samples.

Preparation of Elastic Films from APn-b-EGm-b-APn Samples. Test specimens were prepared as follows. A sample of AP*n*-*b*-EG*m*-*b*-AP*n* was dissolved in DMF. The solution was placed in a poly(tetrafluoroethylene) mold. The solvent was removed in a fume cupboard at 60 °C for an appropriate time, and the residual solvent was then removed at 80 °C under reduced pressure to obtain a flat film of AP*n*-*b*-EG*m*-*b*-AP*n*.

Figure 4-4 shows the DSC data, indicating that the AP*n*-*b*-EG*m*-*b*-AP*n* samples exhibit the glass transition temperatures (T_g) blow 0 °C and no melting point. These observations indicate that the AP*n*-*b*-EG*m*-*b*-AP*n* samples are amorphous and rubbery elastomer at room temperature.

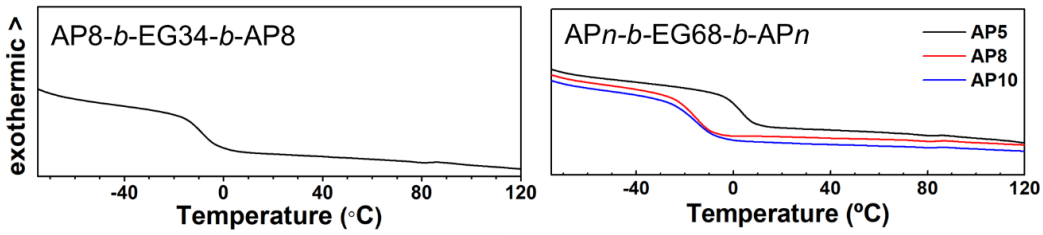

Figure 4-4. DSC profiles of AP8-*b*-EG34-*b*-AP8 and AP*n*-*b*-EG68-*b*-AP*n* copolymers.

As can be seen in Table 4-1, $M_{n,NMR}$ of AP*n*-*b*-EG*m*-*b*-AP*n* samples range (2.8 – 4.6) × 10^3. These molecular weights may be low for elastic properties. However, the flat films prepared by casting showed excellent elastic properties presumably because of dipole–dipole interaction of dense triazole blocks. The inner microstructure of the elastic films formed from AP8-*b*-EG68-*b*-AP8 and AP10-*b*-EG68-*b*-AP10 was characterized by SAXS. Figure 4-5a displays a typical example of SAXS profiles of AP8-*b*-EG68-*b*-AP8 and AP10-*b*-EG68-*b*-AP10. Both the SAXS profiles exhibit a weak but significant signal at q = 0.031 $Å^{-1}$, which corresponds to a regular spacing of 20 nm. It should be noted here that the

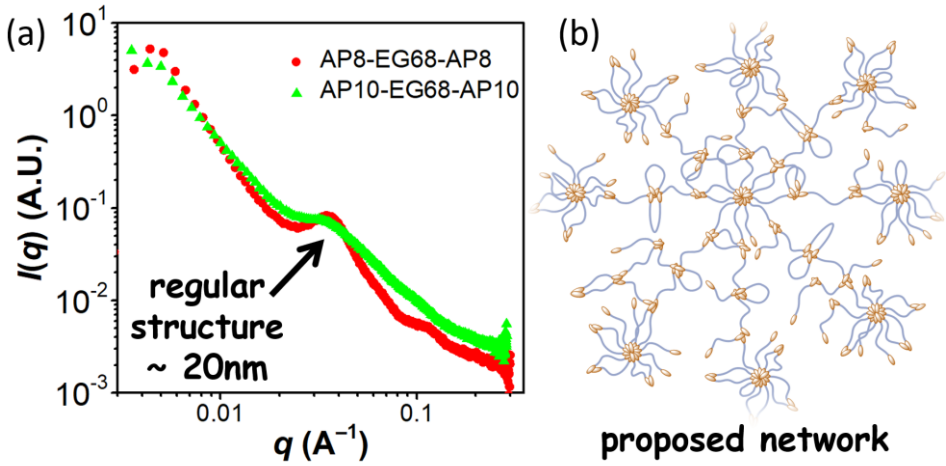

Figure 4-5. SAXS profiles of AP8-*b*-EG68-*b*-AP8 and AP10-*b*-EG68-*b*-AP10 (a), and a proposed network structure (b).

profile of AP8-*b*-EG68-*b*-AP8 also indicate a higher order signal at q = 0.11 Å^{-1}. On the basis of these SAXS profiles, it is concluded that AP*n*-*b*-EG*m*-*b*-AP*n* chains form a regular structure based on microphase separation of EG*m* and AP*n* blocks, in which aggregates of dense triazole blocks act as crosslinks, as illustrated in Figure 4-5b. Since the SAXS profiles contains only a higher order signal presumably because of the broader molecular distribution of AP*n*-*b*-EG*m*-*b*-AP*n* samples, it was not possible to identify the regular structure formed, e.g., hexagonal or body-centered cubic. SAXS measurements were also performed for AP8-*b*-EG68-*b*-AP8 and AP10-*b*-EG68-*b*-AP10 at varying temperatures. The SAXS profiles obtained at 25 and 30 °C were the same for each sample. On

the other hand, the SAXS profiles recorded at 100 °C exhibited a signal at a higher q (= 0.10 Å^{-1}). This observation indicates that the regular structure remains at a temperature as high as 100 °C, but the regular spacing becomes slightly shorter.

Mechanical and Rheological Studies of the APn-b-EGm-b-APn Films. Figure 4-6 presents a typical example of the results of tensile test for AP8-*b*-EG68-*b*-AP8 and AP10-*b*-EG68-*b*-AP10. (The other two samples, AP8-*b*-EG34-*b*-AP8 and AP5-*b*-EG68-*b*-AP5, exhibited lower mechanical strength and stretchability presumably because of shorter EG*m* or AP*n* blocks (data not shown).) The dumbbell shaped specimens of AP10-*b*-EG68-*b*-AP10 exhibited good mechanical strength and stretchability; the rupture strain and stress were ca. 550% and 7.2 MPa at 25 ºC, and 770% and 5.0 MPa at 35 ºC, respectively. From the stress–strain curve in a lower strain region (< 10%), Young's modulus was evaluated to be ca. 29.6 MPa at 25 ºC. The toughness was also calculated to be high from the area of the strain–stress curve, indicative of the strong dipole–dipole interaction of dense triazole blocks. Both the stress–strain curves obtained for the AP8-*b*-EG68-*b*-AP8 and AP10-*b*-EG68-*b*-AP10 samples at 25 ºC contain an initial stiffening region, in which the tensile stress significantly increases with the strain, and exhibit a yield point at a higher strain. After the yield point, the tensile stress decreases and then increases gradually with increasing the strain. These two samples show good stretchability although yield point is seen;

the rupture strains were ca. 400% and 550% for AP8-*b*-EG68-*b*-AP8 and AP10-*b*-EG68-*b*-AP10, respectively. At higher temperatures (30 and 35 °C), the tensile stress increases with the strain, showing no yield point presumably because of higher mobility of chain segments. On the other hand, the tensile stresses are thus reduced and the rupture strains are enhanced. It is noteworthy that Figure 4-6 exhibits different effects of temperature on the mechanical properties for AP8-*b*-EG68-*b*-AP8 and AP10-*b*-EG68-*b*-AP10. In the case of AP8-*b*-EG68-*b*-AP8, the stress–strain curves are different; the tensile stress decreases remarkably with increasing temperature from 25 to 35 °C, whereas the rupture strain increased markedly with temperature. These observations indicate that aggregates of the shorter AP8 blocks, i.e, noncovalent crosslinks, are readily rearranged under stress at higher temperatures. The stress–strain curves for AP8-*b*-EG68-*b*-AP8 at 30 and 35 °C contain a significant signal around 300% strain. At present, the reason for signal is not clear, but it is likely that aggregates of AP8 blocks are considerably rearranged at this strain. In the case of AP10-*b*-EG68-*b*-AP10, on the other hand, the stress–strain curves are almost the same at 30 and 35 °C. It is noteworthy that AP10-*b*-EG68-*b*-AP10 of $M_{n,NMR}$ = 4.6 × 10^3 shows good mechanical properties. These observations indicate that the mechanical properties of AP*n*-*b*-EG68-*b*-AP*n* are more sensitive to temperature for smaller *n*, and the small difference in *n* (8 and 10) is critical for the mechanical properties although the

molecular weight (i.e., *n*) distributions are rather broad.

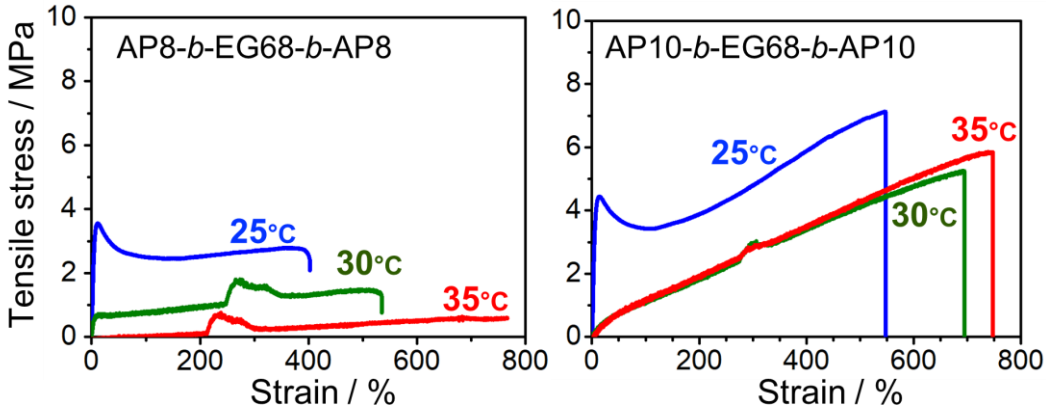

Figure 4-6. Typical examples of strain–stress curves of AP8-*b*-EG68-*b*-AP8 and AP10-*b*-EG68-*b*-AP10 films.

To investigate detail dynamic properties of AP10-*b*-EG68-*b*-AP10, rheology measurements were carried out at varying temperatures with an appropriate strain and varying oscillatory shear frequencies from 0.01 to 100 s^{-1} (Figure 4-7). As shown in Figure 4-7a, both the storage and loss moduli (G' and G'', respectively) decrease with increasing temperature, but G' is always larger than G'' even at 120 °C. This observation also confirms that AP10-*b*-EG68-*b*-AP10 acts as an elastomer in the wide temperature range based on the network structure formed by aggregation of AP10 blocks. By using the time–temperature superposition of rheological data at 25 °C from –25 to 80 °C, a master curve was drawn in Figure

4-7b, which allows ones to see the moduli, G' and G'', over a wide frequency range. This figure demonstrates that the G' values are higher than or equal to G'' values in the whole frequency range from 10^{-8} to 10^{6} s^{-1}. While the superposition does not work in a higher frequency regime at temperatures ≥ 80 °C as shown in Figure 4-7c. This figure shows that G' values decrease with increasing temperature, indicating that the crosslinking density decreases under shear as the temperature increases from 80 to 150 °C. Since the network structure is based on the aggregation of dense triazole blocks, it is likely that the aggregates of AP*n* blocks become less stable under shear at temperatures ≥ 80 °C, as illustrated in Figure 4-7d. It should be noted here that the complex modulus G^* values obtained by rheology measurements are different from Young's modulus obtained by the tensile test. This discrepancy may be caused by reprocessing of the AP10-*b*-EG68-*b*-AP10 sample to prepare films with a proper thickness for rheology measurements.

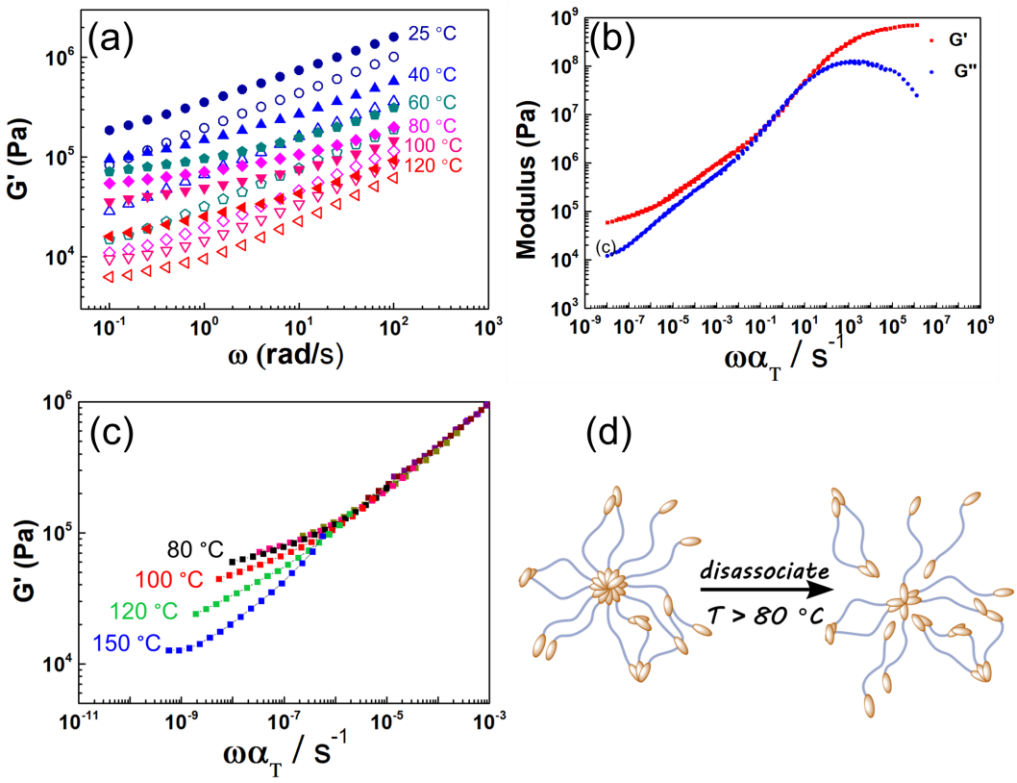

Figure 4-7. Storage and loss moduli, *G′* and *G″*, as functions of angular frequency ω at varying sweeping temperatures (a), the time–temperature superposition curves of *G′* and *G″* at 25 °C from -25 to 80 °C (b), composition curves of *G′* superposed in a high frequency regime at 80, 100, 120, and 150 °C (c), and a conceptual illustration on dissociation of the aggregates of AP*n* blocks at high temperatures under shear (d).

Self-Healing Property. The films formed from AP10-*b*-EG68-*b*-AP10 not only have high stretchability and toughness, but also exhibits good self-healing

capability, because of the network structure based on aggregation of dense triazole blocks. No stretchability and self-healing capacity of common PEG based triblock copolymers, e.g. polystyrene-*b*-poly(ethylene glycol)-*b*- polystyrene (PS-b-PEG-b-PS),[18] [19] were observed. To demonstrate the self-healing capability, a film of AP10-*b*-EG68-*b*-AP10 was cut into two pieces and the cut surfaces were made in contact to allow healing at different times and temperatures. The healed films were then applied the strain–stress measurements at a stretching speed of 1 mm s^{-1}. Figure 4-8 presents the pictures of the AP10-*b*-EG68-*b*-AP10 healed at

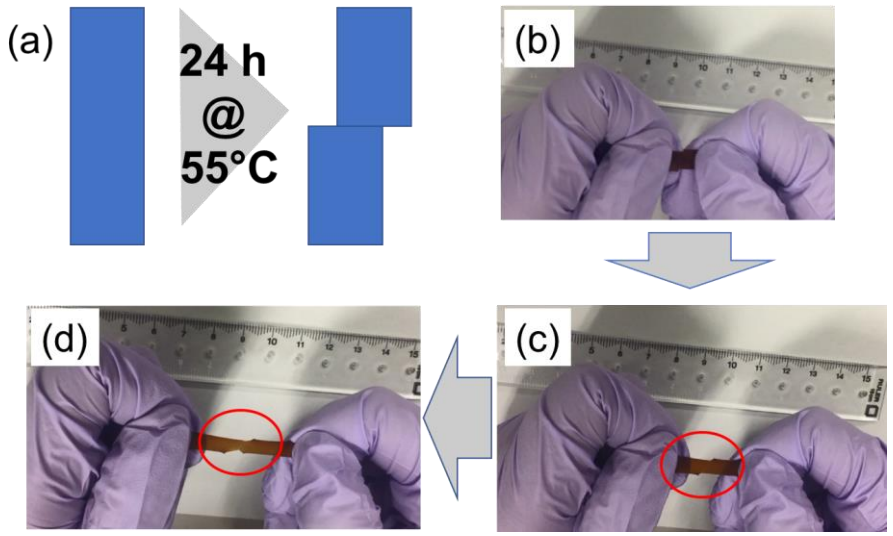

Figure 4-8. Self-healing tests of AP10EG68AP10 films. An illustration of the self-healing experiments, in which the cut surfaces were slightly shifted and brought into contact (a), and photographs of the film of AP10-EG68-AP10 healed at 55 °C for 24 h (b, c, and d). The red circles indicate the heald interface.

55 ºC for 24 h. The two cut surfaces were slightly shifted and brought into contact in a preliminary self-healing experiment to make the healed interface more distinguishable, as illustrated in Figure 4-8a. Figures 4-8b – 4-8d demonstrate that the healed film can be stretched, in which the healed interface is indicated with a red circle. The stress–strain curves for the healed film are compared with that for the virgin sample in Figure 4-9. This figure indicates that the moderate self-healing capability under the present conditions. As expected, the film healed at the higher temperature shows higher rupture stress and strain; Healing at 55 ºC for 24 h led to a recovered rupture strain of ca. 400% and rupture stress of ca. 2.5 MPa. The conditions of self-healing experiments should be optimized to improve the self-healing capability.

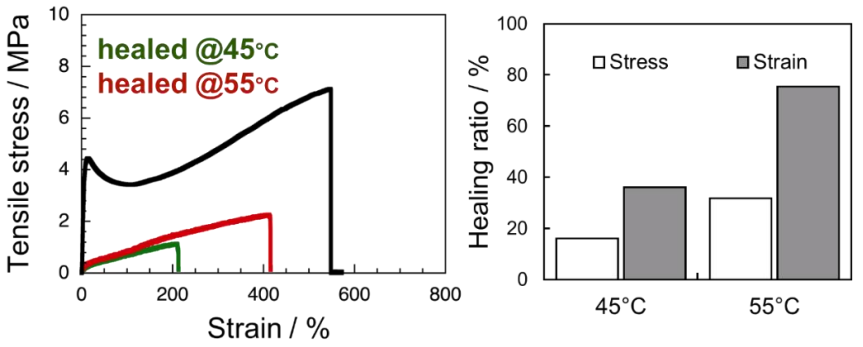

Figure 4-9. Stress–strain curves for the virgin AP10-*b*-EG68-*b*-AP10 film and the films healed at 45 and 55 °C for 24 h (a), and the healing ratio of rupture stress and strain for the healed films (b).

4-4. Conclusion

In this chapter, a new highly stretchable and self-healable material has been developed using the strong dipole–dipole interaction of dense triazole-based blocks. The dense triazole-based systems exhibited distinct characteristics. First, comparing to the other self-healing materials reported to-date, the self-healing AP*n*-*b*-EG*m*-*b*-AP*n* copolymers had the lowest molecular weights $\leq 4.6 \times 10^3$, but possessed robust mechanical properties showing a maximum tensile stress of 7.2 MPa and a strain as high as 770%. The second, the AP*n*-*b*-EG*m*-*b*-AP*n* copolymers showed good self-healing ability. Full-cut fractured AP10-*b*-EG68-*b*-AP10 films reached more than 80% recovery of strain after 24 h at 55 °C. The third is the simple and efficient preparation of the AP*n*-*b*-EG*m*-*b*-AP*n* triblock copolymer compared with other robust materials, which often requires additional synthetic steps. The excellent mechanical and self-healing properties of these copolymers were derived from the rational molecular design of dense triazole blocks, in which individual triazole rings interact cooperatively. The strong intermolecular interaction of AP*n* blocks in turn prompted microphase separation, resulting in enhanced mechanical properties. The author believes that the design concept presented here may represent a general approach to the preparation of new highly stretchable functional materials.

References

(1) Patrick, J. F.; Robb, M. J.; Sottos, N. R.; Moore, J. S.; White, S. R. *Nature* **2016**, *540*, 363−370.

(2) Yang, Y.; Ding, X.; Urban, M. W. *Prog. Polym. Sci.* **2015**, *49*−*50*, 34−59.

(3) Diesendruck, C. E.; Sottos, N. R.; Moore, J. S.; White, S. R. *Angew. Chem. Int. Ed.* **2015**, *54*, 10428–10447.

(4) Yang, Y.; Urban, M. W.; *Chem. Soc. Rev.* **2013**, *42*, 7446–7467.

(5) Binder, W. H. *Self-Healing Polymers: From Principles to Applications*, Wiley-VCH, 2013.

(6) Yanagisawa, Y.; Nan, Y.; Okuro, K.; Aida, T. *Science* **2018**, *359*, 72−76.

(7) Chen, Y.; Kushner, A. M.; Williams, A. G.; Guan, Z. *Nat. Chem.* **2012**, *4*, 467−472.

(8) Kang, J.; Son, D.; Wang, G-J. N.; Liu, Y.; Lopez, J.; Kim, Y.; Oh, J. Y.; Katsumata, T.; Mun, J.; Lee, Y.; Jin, L.; Tok, J. B.-H.; Bao, Z. *Adv. Mater.* **2018**, *30*, 1706846.

(9) Li, C.-H.; Wang, C.; Keplinger, C.; Zuo, J.-L.; Jin, O.; Sun, Y.; Zheng, P.; Cao, Y.; Lissel, F.; Linder, C.; You, X.-Z.; Bao, Z. *Nat. Chem.* **2016**, *8*, 618−624.

(10) Burnworth, M.; Tang, L.; Kumpfer, J. R.; Duncan, A. J.; Beyer, F. L.; Fiore,

G. L.; Rowan, S. J.; Weder, C. *Nature* **2011**, *472*, 334−337.

(11) Lai, J. C.; Jia, X. Y.; Wang, D. P.; Deng, Y. B.; Zheng, P.; Li, C. H., Bao, Z. *Nat. Commun.* **2019**, *10*, 1164.

(12) Appel, E. A.; Biedermann, F.; Rauwald, U.; Jones, S. T.; Zayed, J. M.; Scherman, O. A. *J. Am. Chem. Soc.* **2010**, *132*, 14251–14260.

(13) Liu, J.; Tan, C. S. Y.; Yu, Z. Y.; Li, N.; Abell, C; Scherman, O. A. *Adv. Mater.* **2017**, 29, 1604951.

(14) Liu, J.; Tan, C. S. Y.; Yu, Z. Y.; Li, N.; Abell, C; Scherman, O. A. *Adv. Mater.* **2017**, *29*, 1605325.

(15) Mei, J.-F.; Jia, X.-Y.; Lai, J.-C.; Sun, Y.; Li, C.-H.; Wu, J.-H.; Cao, Y.; You, X.-Z.; Bao, Z. *Macromol. Rapid Comm.* **2016**, *37*, 1667–1675.

(16) Fox, J.; Wie, J.; Greenland, B. W.; Burattini, S.; Hayes, W.; Colquhoun, H. M.; Mackay, M. E.; Rowan, S. J. *J. Am. Chem. Soc.* **2012**, *134*, 5362−5368.

(17) Schulze, B.; Schubert, U. S. *Chem. Soc. Rev.* **2014**, *43*, 2522–2571.

(18) Bouchet, R., Phan, T. N. T., Beaudoin, E., Devaux, D., Davidson, P., Bertin, D., Denoyel, R. *Macromolecules* **2014**, *47*, 2659-2665.

(19) Beaudoin, E., Phan, T. N. T., Robinet, M., Denoyel, R., Davidson, P., Bertin, D., Bouchet, R. *Langmuir* **2013**, *29*, 10874-10880.

Chapter 5

Conclusions

In this study, new block copolymers possessing poly(ethylene glycol) and dense 1,2,3-triazole blocks have been prepared. Various properties and functions of these copolymers were systematically investigated.

In Chapter 2, diblock copolymers diblock copolymers, EG*m*-*b*-AP*n* and EG18-*b*-AB7, possessing a dense 1,2,3-triazole block were successfully prepared by CuAAC polymerization of AP and AB, respectively, in the presence of EG*m*-P. All the EG*m*-*b*-AP*n* and EG18-*b*-AB7 copolymer samples were well soluble in water. The self-association behavior in water was studied. Interestingly, the author has found that the dense 1,2,3-triazole blocks act as hydrophobe in water, although 1,2,3-triazole ring has a large dipole moment and can form hydrogen bonding. The reason may be the strong dipole–dipole interaction offered by the dense 1,2,3-triazole rings. Various self-assembled nanostructures in water were obtained, i.e., spherical micelles, vesicles, and cylindrical micelles even with relatively short dense 1,2,3-triazole blocks, e.g., EG18-*b*-AP4 and EG45-*b*-AP6. Moreover, the self-assemblies formed from EG18-*b*-AP10, EG45-*b*-AP14, and EG18-*b*-AB7 underwent further aggregation at higher temperatures, which showed thermoresponsive properties. The thermoresponsive association behavior

can be controlled by the relative block length and composition of dense 1,2,3-trizole blocks.

In Chapter 3, the solubility and photophysical properties of EG*m*-*b*-AP*n* in solution state were investigated. The incorporation of EG*m* block significantly enhanced the solubility of bock copolymers in common polar solvents. Increasing the length of AP*n* block, the solubility decreased in these solvents. Unexpectedly, the block copolymers emitted fluorescence in solution state. The emission of block copolymers was tuned from ultraviolet to green fluorescence by changing the excitation wavelength. This emission behavior may be based on the polydispersity of copolymers. PGSE NMR analysis and theoretical calculation have indicated that the copolymers are molecularly dispersed in DMF-d_7 and AP*n* block is an intrinsic fluorophore. Finally, the emission responsive property of block copolymer to metal ions was studied because of the interaction with dense 1,2,3-triazole blocks dependent on the ionic species.

In Chapter 4, the author prepared BAB type dense 1,2,3-triazole-based triblock copolymers, AP*n*-*b*-EG*m*-*b*-AP*n*. Using the strong dipole–dipole interaction of dense triazole-based blocks, new strong and highly stretchable elastomer with good self-healing ability was developed. This new dense triazole-based elastomer exhibited distinct characteristics. To the best of the author's knowledge, this self-healable AP*n*-*b*-EG*m*-*b*-AP*n* copolymer had the lowest

molecular weights ≤ 4.6×10^3, but with strong mechanical properties possessed a maximum tensile stress of 7.2 MPa and a strain as high as 770%. Moreover, the preparation of these copolymers was simple, robust, and efficient. No requirements of tedious synthetic steps, specific chemicals, and harsh experimental condition were required. The excellent mechanical and self-healing properties of these copolymers resulted from two factors; (1) rational molecular design of dense triazole blocks, in which individual triazole rings interact cooperatively, and (2) the presence of microphase separation. The strong intermolecular interaction of AP*n* blocks caused microphase separation, which in turn enhanced mechanical properties.

In conclusion, the author successfully synthesized new 1,2,3-triazole-based diblock and triblock copolymers. The copolymers are soluble in some common solvents. The properties and functions of these new copolymers were investigated. The author believes that this work presented here will afford a new aspect for fabricating new novel triazole-based functional materials.

List of Publications

The contents of this thesis have been published or will be published in following papers:

(1) Yang, Y.; Hashidzume, A. Synthesis of New Diblock Copolymers of Poly(ethylene glycol) and Dense 1,2,3-Triazole Blocks: Self-Association Behavior and Thermoresponsive property in Water. *Submitted* (Chapter 2)

(2) Yang, Y.; Mori, A.; Hashidzume, A. Emission Properties of Diblock Copolymers Composed of Poly(ethylene glycol) and Dense 1,2,3-Triazole Blocks. *Polymers,* **2019**, *11*, 1086. (Chapter 3)

(3) Yang, Y.; Hashidzume, A. Tough and Strong Self-Healing Elastomer Formed from Triblock Copolymers Possessing Dense 1,2,3-Triazole Blocks. *In preparation* (Chapter 4)

Other Papers

(1) Yu, F.; Yang, Y.; He, D.; Gong, D.; Chen, Z.-R., Pressure-Sensitive Supported FI Catalyst for the Precise Synthesis of Uni- and Bimodal Polyethylene, *Ind. Eng. Chem. Res.* **2017**, *56*, 4684–4689.

(2) Tan, D.; Tu, S.; Yang, Y.; Patskovsky, S.; Rioux, D.; Meunier, M., Engineering of Host–Guest Interactions To Tune the Assembly of Plasmonic Nanoparticles, *J. Phys. Chem. C* **2016**, *120*, 21790–21796.

(3) Yang, Y.; Yu; F.; Huang, L.; Chen, Z. R., A Facile Approach to Control Metal Superstructure Architecture with Organic Thin Films, *RSC Adv.* **2016**, *6*, 7409–7423.

(4) Wang, W.; Ren, G.; Yang, Y.; Cai, W.; Chen, T., Synthesis and Properties Study of the Uniform Nonspherical Styrene/Methacrylic Acid Copolymer Latex Particles, *Langmuir* **2015**, *31*, 105–109.

(5) Yang, Y.; Wang, W.; Chen, T.; Chen, Z.-R., Simultaneous Synthesis and Assembly of Silver Nanoparticles to Three-Demensional Superstructures for Sensitive Surface-Enhanced Raman Spectroscopy Detection, *ACS Appl. Mater. Interfaces* **2014**, *6*, 21468–21473.

(6) Cai, W.; Wang, W.; Yang, Y.; Ren, G.; Chen, T., Sulfonated Polystyrene Spheres as Template for Fabricating Hollow Compact Silver Spheres *via* Silver–Mirror Reaction at Low Temperature, *RSC Adv.* **2014**, *4*, 2295.

(7) Ren, G. H.; Wang, W.; Yang, Y.; Cai, W.; Chen, Z.-R., Coating Polypyrrole-Silver Nanocomposites on Sulfonated-Polystyrene Microspheres by One-

Step Method Using $AgNO_3$ as an Oxidant, *J. Polym. Mater.* **2014**, *31*, 135–144.

(8) Wang, W.; Cai, W.; Yang, Y.; Li, H.; Cong, M.; Chen, T., Controlled Growth of Metal Nanoparticles on Amino-Functionalized Polystyrene Microspheres And Their Application in Surface-Enhanced Raman Spectroscopy, *Mater. Chem. Phys.* **2013**, *142*, 756.